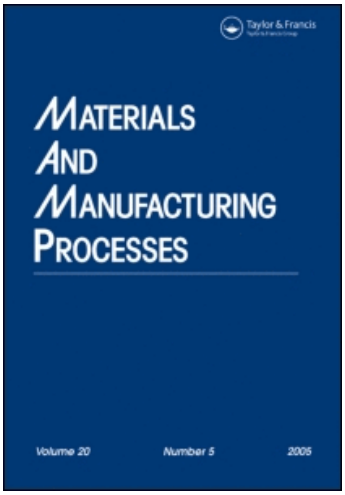

Materials and Manufacturing Processes
Publication details, including instructions for authors and subscription information:
http://www.informaworld.com/smpp/title~content=t713597284

DNA Functionalized Carbon Nanotubes for Nonbiological Applications

Ambarish Paul[a]; Baidurya Bhattacharya[b]
[a] Advanced Technology Development Centre, IIT Kharagpur, Kharagpur, India [b] Civil Engineering Department, IIT Kharagpur, Kharagpur, India

Online publication date: 08 September 2010

To cite this Article Paul, Ambarish and Bhattacharya, Baidurya(2010) 'DNA Functionalized Carbon Nanotubes for Nonbiological Applications', Materials and Manufacturing Processes, 25: 9, 891 — 908
To link to this Article: DOI: 10.1080/10426911003720755
URL: http://dx.doi.org/10.1080/10426911003720755

Materials and Manufacturing Processes, 25: 891–908, 2010

ISSN: 1042-6914 print/1532-2475 online
DOI: 10.1080/10426911003720755

Taylor & Francis
Taylor & Francis Group

DNA Functionalized Carbon Nanotubes for Nonbiological Applications

AMBARISH PAUL[1] AND BAIDURYA BHATTACHARYA[2]

[1]*Advanced Technology Development Centre, IIT Kharagpur, Kharagpur, India*
[2]*Civil Engineering Department, IIT Kharagpur, Kharagpur, India*

Functionalization of an inorganic nanomaterial like carbon nanotube (CNT) with biological macromolecules like deoxyribonucleic acid (DNA) leads to the formation of hybrid materials with fascinating properties. This article describes the structures of CNT and DNA, portrays the van der Waals force-dominant non-covalent π–π stacking interactions formed due to their self-assembly, and reviews the electronic, electrochemical, optical, and chemical properties of DNA-functionalized CNTs (DFCs). Current computational developments in simulating and predicting CNT-DNA interactions, alternate functionalization techniques, conformational changes of DNA bases, etc. are discussed. Various characterization techniques using scanning electron microscopy (SEM), scanning tunneling microscopy (STM), atomic force microscopy (AFM), UV-visible, Photoluminescence (PL) and Raman spectroscopy, etc. that help explain DFC properties are detailed. Potential applications for this hybrid material in nanoelectronics and chemical sensors as well as in chirality-based separation of metallic nanotubes from semiconducting ones are considered. The article concludes with current challenges, future directions of research, and prospective applications in this field.

Keywords Carbon nanotube; Characterization; Deoxyribonucleic acid; Functionalized; Non-covalent; Sensors.

LIST OF ABBREVIATIONS

1. AFM: Atomic Force Microscopy
2. ALD: Atomic Layer Deposition
3. CD: Circular dichroism
4. CHARMM: Chemistry at HARvard Macromolecular Mechanics
5. CNT: Carbon nanotubes
6. COM: Centre of Mass
7. CV: Cyclic Voltammetry
8. CVFF: Consistent Valence Force Field
9. DFTB: Density functional based tight binding
10. DFC: DNA functionalized CNT
11. DMMP: dimethyl methylphosphonate
12. DNA: Deoxyribonucleic acid
13. DNT: dinitrotoluene
14. DOS: Density of States
15. dsDNA: double stranded DNA
16. EDC: 1-ethyl-3-(3-dimethylaminopropyl) carbodiimide hydrochloride
17. EIA: Electrochemical Impedance Analysis
18. FET: Field effect transistor
19. GROMACS: GROningen MAchine for Chemical Simulations
20. HiPCO: High pressure carbon monoxide
21. ICD: Induced Circular Dichroism
22. IEC: Ion–Exchange Chromatography
23. LD: Linear dichroism
24. L-CPL: Left-handed circularly polarized light
25. MD: Molecular Dynamics
26. MWNT: Multi-walled carbon nanotube
27. NHS: N-hydroxy-succinimide
28. NIL: Nanoimprint lithography
29. OPLSAA: Optimized Potential for Liquid Simulations-All Atoms
30. PL: Photoluminescence
31. PLE: Photoluminescence excitation
32. PSD: Position Sensitive Detector
33. RBM: Radial breathing mode
34. R-CPL: Right-handed circularly polarized light
35. RRS: Resonant Raman Spectroscopy
36. SDS: Sodium dodecyl sulfate
37. SEC: Size Exclusion Chromatography
38. SEIRA: Surface Enhanced Infrared Absorption
39. SEM: Scanning Electron microscopy
40. ssDNA: Single stranded DNA
41. STM: Scanning Tunneling Microscopy
42. SWNT: Single walled carbon nanotube
43. TIP3P: Transferable Intermolecular potential-3 point
44. TMA: trimethylamine
45. UV: Ultraviolet
46. UV-vis: UV-visible

INTRODUCTION

Since the discovery of carbon nanotubes (CNTs) in 1991 by Ijima [1], they have found extensive applications in a wide cross-section of disciplines because of their fascinating and versatile properties. Over the past five years, there has been a burst of research activities on bio-modified CNTs for technological applications. Biological functionalization, especially deoxyribonucleic acid (DNA) functionalization (Fig. 1), has attracted much scientific interest due to the possible development of sensitive and ultrafast detection systems for molecular electronics. Due to the presence of a large number of delocalized π-electrons on its bases, DNA can be used as molecular wire. Both CNT [2] and DNA [3] were separately used to bridge the

Received September 24, 2009; Accepted January 26, 2010
Address correspondence to Baidurya Bhattacharya, Civil Engineering Department, IIT Kharagpur, Kharagpur 721302, India; Fax: +91-3222-282254; E-mail: baidurya@iitkgp.ac.in

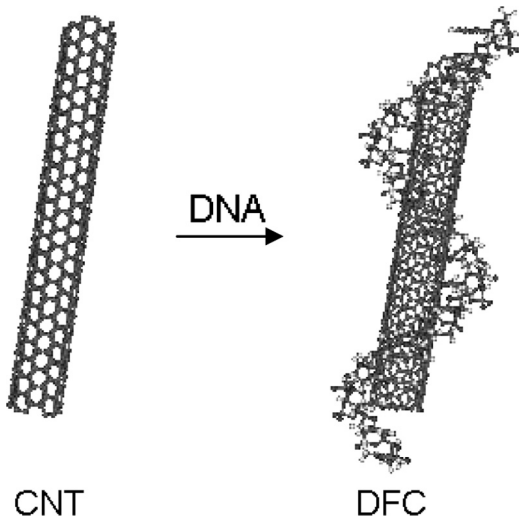

FIGURE 1.—Schematic of DNA functionalized CNT (DFC).

nanometer gap between nanoelectrodes patterned on silicon dioxide support. Recent techniques have facilitated gap size monitoring in real time by scanning electron microscopy (SEM) during the fabrication of nanoelectrodes [4]. It has been observed that I–V characteristics of such field effect transistors (FETs) are greatly dependent on the gate voltage and that the bridging double stranded DNA (dsDNA) molecule acted as a *p*-type channel between source and drain electrodes [5]. Since DNA provides a negative charge to the substrate to which it attaches, end-functionalized CNT can be aligned by depositing it between metal electrodes [6]. Alignment of CNT has also been achieved by functionalizing the nanotubes with DNA and then aligning them through a passing meniscus [7]. Alignment of CNTs in composites enhances their mechanical strength. Since DNA binds to CNT via non-covalent bonding resulting from stacking interactions, the mechanical properties of the DNA-modified CNT-composite films may not generate high mechanical strength. However, DNA-functionalized single-walled carbon nanotube (SWNT) could form conductive films that could be used in space applications demanding transparent films to minimize solar absorbance; the use of higher weight percentage of CNTs should lessen the transparency of composite films. Because of their large surface area and rich π-electron conjugation on their outer surface, CNTs were seen to be electrochemically active. DNA modification of the surface of CNTs may lead to varied adsorption of chemical moieties, permitting their use in sensing or detection of chemical radicals. DNA assisted self-assembling of CNTs can be utilized in the construction of assembled miniature multi-nanotubes structures for multifunctional material and device applications [8].

With DNA functionalized CNT field effect transistors (DFC-FETs), subthreshold swing as low as 60 mV/decade was achievable thus facilitating the operation of devices that work at low voltages [9]. DFC could prove itself as a component of future generation high performance electronic devices because of its superior electrical transport properties, chemical robustness, and lack of surface dangling bonds.

As a hybrid material DFC can potentially revolutionize molecular electronics. The properties of this hybrid material depend on the structure of individual entities, i.e., both the CNT and the DNA as well as on the nature of the interaction between them. Section 2 is devoted to the study of the structure of single stranded DNA (ssDNA) and the structure of the CNT separately and the interaction between them in a self-assembled bio-modified material. Section 3 discusses the computational developments using molecular dynamics (MD) for the study of this complex structure and predict some of its useful properties, namely, electrochemical properties, chemical properties, electronic properties, dispersion and solubility in water, and vibrational properties, which are the subject of Section 4. Section 5 focuses on the characterization techniques frequently used for DFC, including Raman spectroscopy, SEM, scanning tunneling microscopy (STM), AFM, ultraviolet (UV) spectroscopy, fluorescence and photoluminescence (PL) investigations, linear dichroism (LD), and circular dichroism (CD). Section 6 deals with possible applications of DFCs including chemical sensors, FETs, and in chirality-based separation of CNTs.

STRUCTURE OF DNA FUNCTIONALIZED CNT (DFC)

Structure of DNA

The function of a biological or non-biological moiety strongly depends on its structure. In order to understand and modify a biological structure such as that of DNA, it is necessary to analyze each of its components. DNA is a polymer with deoxyribonucleotides as its repeating or monomeric units. Each monomer unit is made up of three parts, namely, a phosphate group, a furanose sugar moiety, and one of the four possible nitrogenous bases: adenine (A), guanine (G), cytosine (C), or thymine (T).

The acidity of the nucleic acid results from the distribution of a lone negative charge amongst the two pendant oxygen atoms in the PO_4^- group that constitutes the "rigid backbone" of the polynucleotide entity. As a part of this entity, the P–O bonds, which form a tetrahedron around the phosphorous (P) atom, are elongated by 0.2 Å.

The furanose moiety consists of a five-membered ring with exocyclic alcohol and hydroxyl groups attached to it. In order to avoid short contacts between the pendant hydrogen (H)-atoms of the $HO–CH_2–C^{ring}–H$ entity, the furanose ring is puckered into an energetically favorable conformation as shown in Fig. 2. The planar nitrogenous bases can be composed of either purines or pyramidines, which, however, have no internal flexibility. Guanine and adenine are the purines (Fig. 3), whereas the cytosine and thymine form the pyramidine class (Fig. 4).

Each base is linked to the sugar through a covalent glycosidic bond to form a nucleoside (Fig. 5). The plane of the base is almost perpendicular to the plane of the sugar ring. The phosphate group bonds with the sugar covalently to form a mononucleotide and also increases conformational possibilities. Mononucleotides are linked to each other through phosphodiester bonds [Figs. 6(a) and (b)] to form a polynucleotide.

Double stranded DNA consists of two single strands of polynucleotide twirled together, connected by pairs of

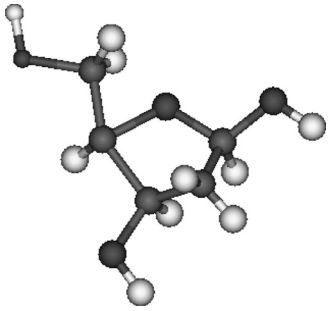

FIGURE 2.—Structure of sugar furanose. The grey, white, and red balls represent carbon, hydrogen, and oxygen atoms, respectively.

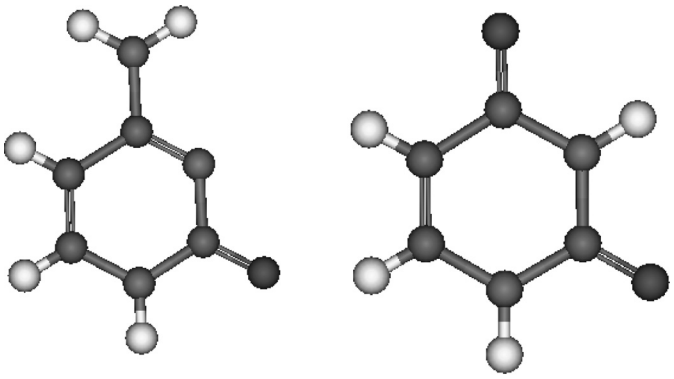

(a) (b)

FIGURE 4.—Structure of pyramidine bases: (a) cytosine (C) and (b) thymine (T). The grey, white, blue, and red spheres represent carbon, hydrogen, nitrogen, and oxygen atoms, respectively.

complementary nitrogenous bases forming a ladder with rung arrangement with the two strands arranged antiparallel to each other (Fig. 7). A and T and G and C form base pairs, respectively, due to energetically favorable hydrogen bonding schemes, as the complementary base pairs are of the same size. Each purine base pairs up with its respective complementary base through hydrogen bond (H-bond) formed between the electronegative oxygen (O)-atom of the purine or the pyramidine base and the H-atom linked to the nitrogen (N)-atom of the bases. A and T are paired up via two H-bonds [Fig. 8(a)] and G and C are paired up through three H-bonds [Fig. 8(b)] depending on the availability of H-bond formation sites. Such arrangements of base pairing minimize the energy of the inter-twirled structure. Hence the complementary bases are defined with respect to the H-bonding scheme between the bases. Any cross-pairing would lead to distortion in the double helix structure and is not energetically favorable. The furanose–phosphate chain of the polynucleotide backbone forms the side of the ladder, where the base pairs are placed perpendicular to the axis. These aromatic purine or pyramidine rings consist of π-lobes extending from their atoms. Since the π-electron lobes of the nucleotide bases extend above and below the rungs of the ladder, the lobes overlap with the π-electron counterparts from neighboring rungs.

As the aromatic rings of the nucleotide bases in a DNA molecule are positioned nearly perpendicular to the helical axis of the strands, the faces of the aromatic rings are arranged parallel to each other, allowing the bases to participate in aromatic interactions [10]. Thus the π-orbital of the aromatic rings of a pair of complementary bases are stacked over each other resulting in π-stacking interactions. These interactions are mostly van der Waals and electrostatic [11] interactions but collectively are strong forces due to the sum of all π-stacking interactions within DNA. In this way, net stabilizing energy is provided to the molecule. Such bonds are termed as non-covalent bonds and are individually weaker than covalent bonds.

The π-electrons being delocalized form a continuous conductive pathway through the molecule often termed as the π-way [12]. A similar case applies to single stranded DNA (ssDNA) referred to as a molecular wire because of the presence of π stacked [13, 14] delocalized electrons around the complementary bases. MD simulations have shown that the ssDNA has many degrees of freedom and a rugged free-energy landscape containing many local minima [15].

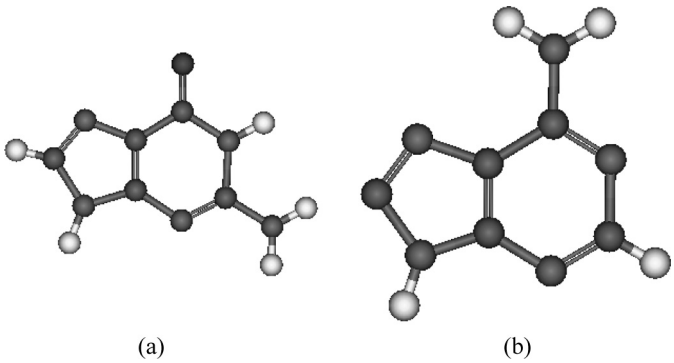

(a) (b)

FIGURE 3.—Structure of purine bases: (a) guanine (G) and (b) adenine (A). The grey, white, blue, and red spheres represent carbon, hydrogen, nitrogen, and oxygen atoms, respectively.

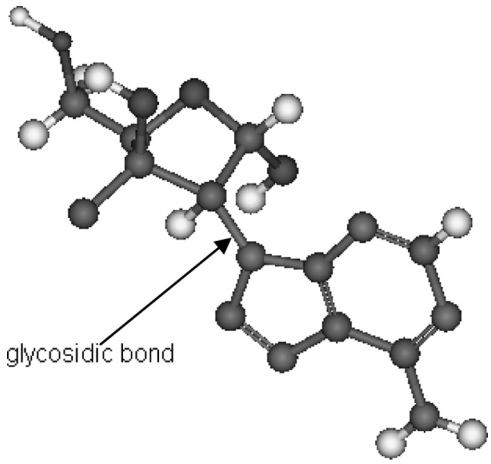

FIGURE 5.—Glycosidic bond between sugar and base. The grey, white, blue, and red spheres represent carbon, hydrogen, nitrogen, and oxygen atoms, respectively.

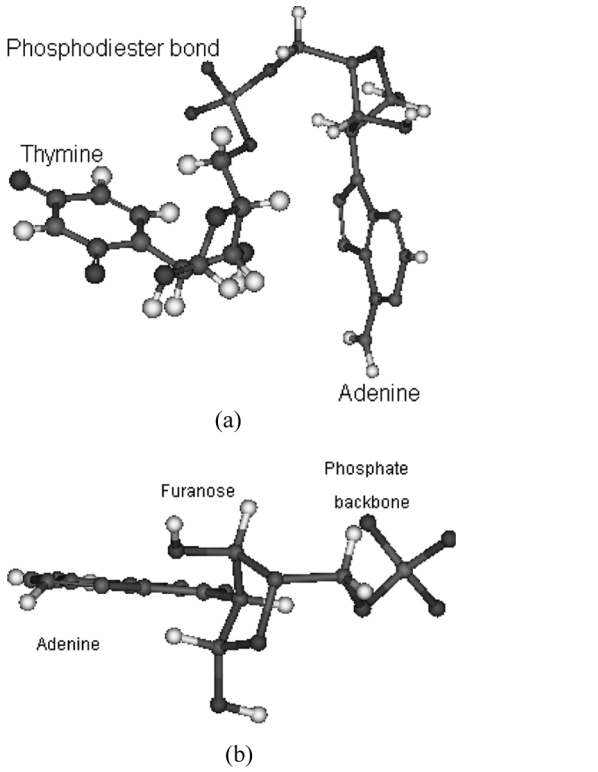

FIGURE 6.—Bonding of mononucleotides of thymine and adenine to form polynucleotide. The mononucleotides link to each other through phosphodiester bonds. (b) Adenine mononucleotide links itself to the phosphate group (backbone). Note that the plane of the nitrogenous base (adenine in this case) is perpendicular to the plane of the furanose ring. The grey, white, blue, orange, and red spheres represent carbon, hydrogen, nitrogen, phosphorus, and oxygen atoms, respectively.

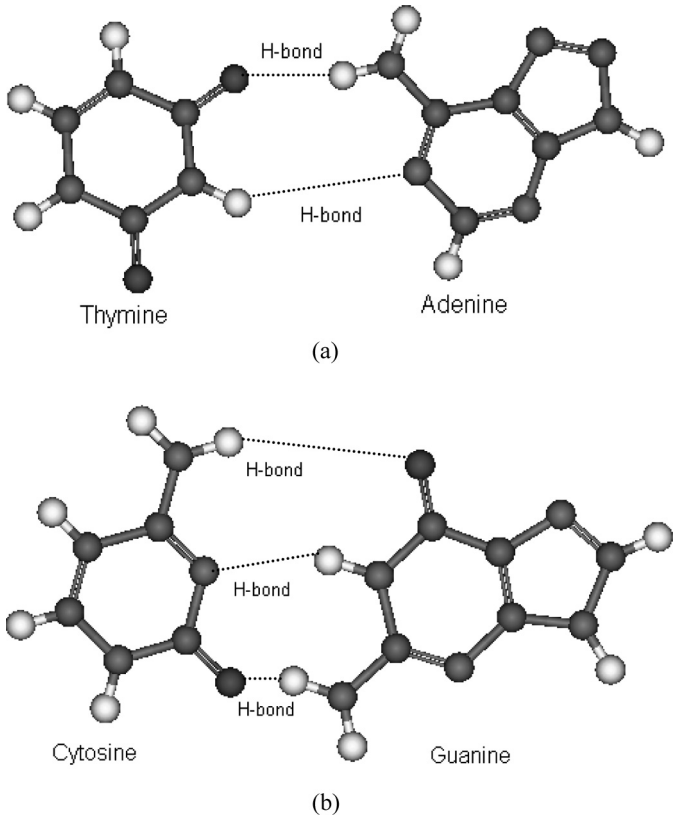

FIGURE 8.—Complementary base pairing in nucleic acids of DNA: (a) adenine (A) pairs with its complementary base thymine (T) via two hydrogen bonds (H-bonds) forming A-T base pair and (b) guanine (G)) pairs with its complementary base cytosine (C) via three hydrogen bonds (H-bonds) forming G-C base pair. The grey, white, blue, and red spheres represent carbon, hydrogen, nitrogen, and oxygen atoms, respectively.

Structure of CNT

A CNT can be considered as a unique 1-D hollow nanostructure resembling a quantum wire, where the building block consists of an all-carbon, one-atom thick cylindrical tube called the SWNT, typically having a high aspect ratio (length-to-diameter ratio). Multi-walled nanotubes (MWNTs) are best described as coaxially arranged SWNTs with regularly increasing diameters according to the Russian doll Model (Fig. 9). A CNT can be visualized as a rolled-up graphene sheet containing hexagonal rings of C-atoms with dome-shaped end-caps. The curvatures of the end-caps are brought about by the presence of pentagonal rings considered as topological defects [16] in the otherwise hexagonal structure of the lattice. Firstly, the pentagons give a convex curvature to the edge of the tube which helps in closing the tube. Secondly, the pentagonal ring induces defects on the end-caps of the tube making the end-caps chemically active, and a chemical moiety is likely to be anchored at the defect site of the cap

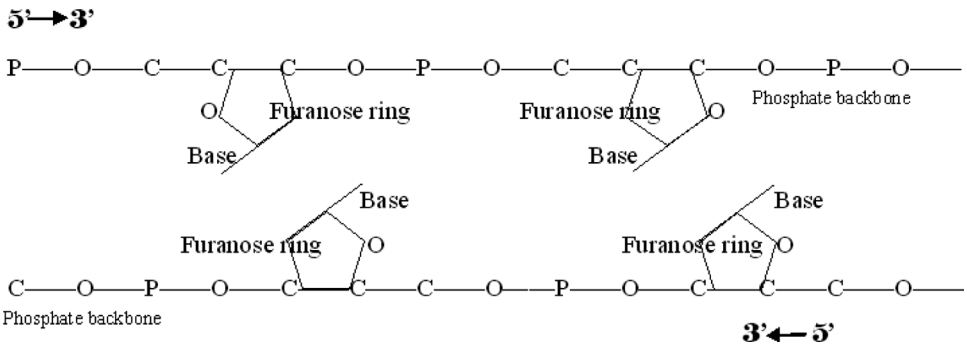

FIGURE 7.—Schematic arrangement of antiparallel strands of DNA.

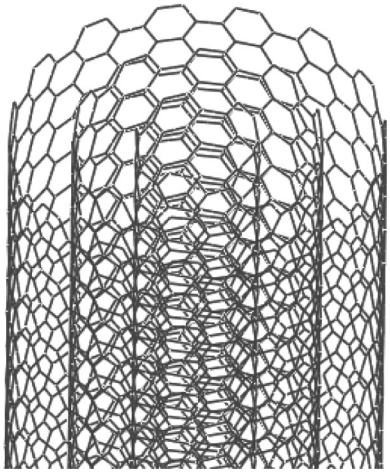

FIGURE 9.—Schematic representation of the Russian Doll Model.

[17]. However, chemical reactivity of the nanotube surface also depends on its natural and strain-induced curvature [18]. Opening of the end-caps of CNT to end-functionalize them is required for various applications and is achieved by acid (HNO_3) treatment [19–22], vapor phase oxidation [23], plasma etching [24], and argon plasma assisted UV grafting [25].

The nomenclature (n, m) is used to identify each SWNT, which can be uniquely characterized by the vector $\vec{C}$ in terms of integers n and m corresponding to graphite vectors $\vec{a}_1$ and $\vec{a}_2$ as $\vec{C} = n\vec{a}_1 + m\vec{a}_2$. Nanotube type (n, n), $(n, 0)$, and (n, m) are called arm-chair [Fig. 10(a)], zigzag [Fig. 10(b)], and chiral nanotubes [Fig. 10(c)], respectively, and depends on the rolling direction of the graphene sheet. This rolling of the graphene sheet into tubular structures determines the unique electronic behavior of the CNT, due to which some CNTs behave as metals and some as semiconductors. It can be further noted that when the integer p $(=n - m)$ is a multiple of 3, the CNT shows metallic behavior whereas the rest of the CNTs behave as semiconducting [26]. Thus in a given sample one-third of the CNTs can be expected to show metallic behavior.

The partial rehybridization of the C-atom from sp^2 to sp^3 hybridized state in the CNT, accounting for its curvature, brought about by $\sigma - \pi$ mixing, together with π-electron confinement, imparts unique electronic, chemical, mechanical, and optical properties to the nanotubes. The C-atoms in graphene sheet have π orbital on either side of the plane. Because of the curvature of the CNT the electron clouds are no longer uniformly distributed as in graphene sheet [Fig. 11(a)] but forms an asymmetric distribution of π-lobes inside and outside the cylindrical sheet of CNT [Fig. 11(b)]. Due to the distorted electron cloud, a rich π-electron conjugation is formed on the outer surface of the CNT, which makes it potentially applicable for chemical sensors. Electron-donating and electron-withdrawing chemical moiety can result in electron transaction to or from the π-electrons of CNT.

The challenge behind the commercial use of CNT lies in the proper segregation and isolation of individual CNTs.

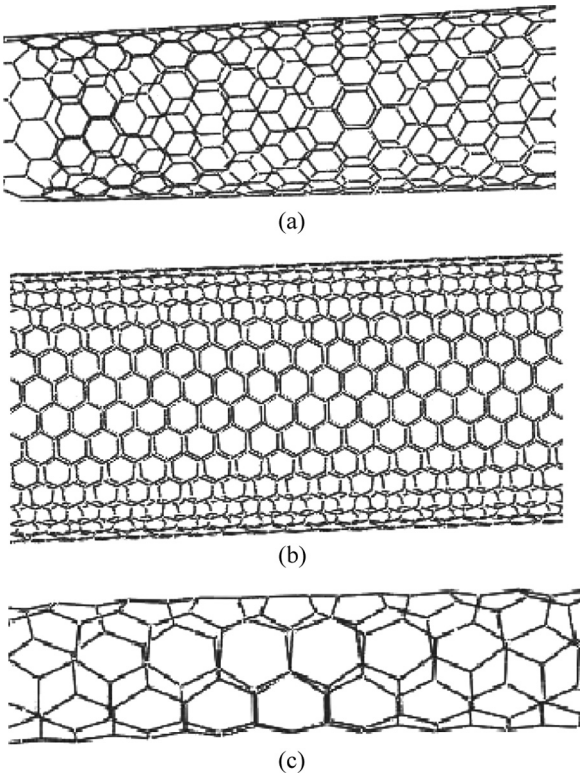

FIGURE 10.—Types of carbon nanotubes (a) arm-chair (b) zigzag, and (c) chiral nanotube with chiral angle of around 25°.

Zheng and coworkers [14] first showed the dispersion of CNT through functionalization with DNA. The researchers used a suspension of high pressure carbon monoxide (HiPCO) CNT in aqueous solution of DNA with NaCl, sonicated for 90 min in an ice-cold water bath and centrifuged to remove the insoluble materials. Jeng and coworkers [27] described a novel route to attach ssDNA to the sidewalls of CNTs and then remove the free standing DNA from the solution by a process of high molecular

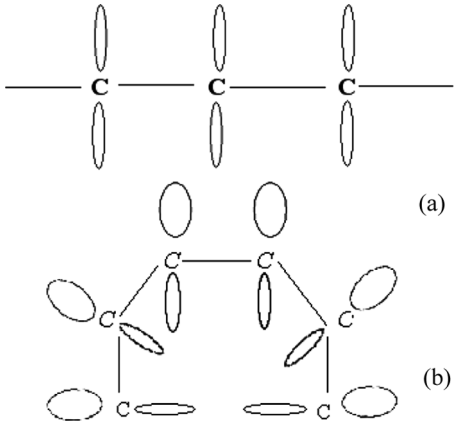

FIGURE 11.—Schematic of electron distribution of (a) plane graphene and (b) CNT.

weight dialysis for 48 hours. This resulted in the removal of 95% of the free floating DNA as observed in UV spectra.

Interaction of CNT with DNA

Strong interactions between DNA and CNT had been reported as early as 1997 by Tsang and coworkers [28]. The nucleosides of DNA interact with CNT predominantly through van der Waals forces and forces arising as a result of mutual polarization of the molecules in close proximity to each other, changing the electronic structure of the system [29]. However, through density functional based tight binding (DFTB) calculations, Enyashin and coworkers [30] asserted that the interaction is not strictly van der Waals as it involves a couple of mixed states which appear below the Fermi level. Meng and coworkers [29] in 2007 measured the interaction of the bases with the CNT and, thereby, observed the local electronic states of the robust system by a sensitive stationary STM tip. The DNA interacts with the CNT through their base unit of the nucleosides placed at a distance of 3.3 Å away from the wall of the CNT. As mentioned earlier the bases are rigid structures and do not undergo conformational changes, but the sugar residue which is farther away from the CNT, owing to its orientation flexibility, usually has its major part of the plane of the puckered pentagonal ring perpendicular to the CNT wall with the oxygen (O) atom of the –OH moiety, attached to ring, pointing towards it (Fig. 12).

Though N-, C-atoms of adenine are found to occupy the hollow sites of the graphene hexagonal ring [31], the same arrangement is not found in the curved wall of the CNT, where these atoms sits in such positions that maximize the van der Waals force of attraction between the N-, O-, and C-atoms of the base and the C-atom of CNT. Because of the asymmetric structure of the CNT along its tube axis, the most dominant orientation of bases upon adsorption to the CNT surface are those with the sugar-base direction pointing perpendicular to the tube axis or slightly tilted to it. This geometry is most favorable for the wrapping of ssDNA [14] on the CNT as has been confirmed by simulations [32].

The wrapping of the ssDNA around the CNT [10, 13] is brought about by the interaction forces generated from the π-orbital overlap (stacking) between the DNA and the CNT. This stacking causes a high density of delocalized electrons around the DNA-CNT hybrid system that facilitates conduction of electrons. Zheng and coworkers [14] showed that ssDNA of the poly-d(GT) sequence forms a stable complex with individual CNTs by wrapping around them via the aromatic interactions between the G and T bases and the sidewall of the CNT resulting in a strong interaction [33]. MD simulations has also confirmed that the DNA binds to CNTs via π-stacking [34, 35].

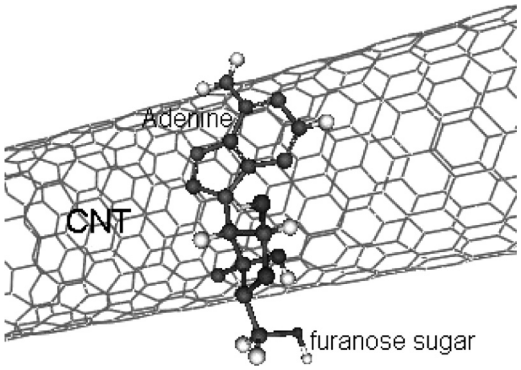

FIGURE 12.—Interaction of adenine with (10, 0) CNT. The grey, blue, red, and white spheres represent C, N, O, and H atoms, respectively.

COMPUTATIONAL DEVELOPMENTS

Computational tools have played a pivotal part in the prediction of properties of complex systems. MD simulation that calculates the time dependent behavior of a molecular system has proved to be one of the principal tools in the theoretical study of nanoscale systems [36] and design of new materials [37, 38]. It has provided detailed information about the dynamics of CNT and also on the fluctuations and conformation changes in a variety of bio-molecules like DNA and protein. Efforts have been made to investigate the interaction dynamics of CNT with DNA, the electronic properties of the hybrid structures, and also the chemical association responsible for the formation of self assembled structures.

MD simulations have predicted an alternative way to functionalize CNT [39]. This has been done by inserting ssDNA oligonucleotides in CNT capsule suspended in a water soluble environment, mediated by combined van der Waals and hydrophobic forces. The study was carried out with DNA oligonucleotides with 8 adenine bases and a (10, 10) CNT, solvated in aqueous medium. The system was simulated for 2 ns at a temperature of 400 K and a pressure of 3 bars with a time-step of 1 fs and a full-precision trajectory recorded every 1 ps. The DNA was inserted into the nanotube by repelling of water molecules from the tube, which required an energetically triggered process. It was asserted that the oligonucleotides and the nanotube experienced attractive van der Waals forces when they were in the range of 1 nm or less. The work also discusses the interfacial interaction between the DNA bases, the CNT and the H-bonds of water. Computer simulations were conducted where DNA oligonucleotides were inserted into the CNT junctions by induced pressure gradient by pushing a layer of water molecules towards the flow direction to drive in the DNA oligonucleotide [40]. Investigations were performed to study the flow characteristics of DNA oligonucleotide and water molecule through CNT nanochannels under induced pressure. It was observed that the DNA oligonucleotide cannot be transported through the (8, 8)-(12, 12) CNT junction channel but can be translocated through the (10, 10)-(14, 14) CNT junction channel by pressure gradient. The insertion depth of the oligonucleotides into the nanochannel depends on the induced pressure and on the conformation of the molecule. Using MD simulations performed with Chemistry at HARvard Macromolecular Mechanics (CHARMM) force fields, Lau and coworkers [41] studied the structural effects of the confinement of double stranded DNA within a hydrophobic CNT and found that the DNA bends away from the closest nanotube wall and even the less polar bases of the nucleic acid, which should have interacted

with the nanotube wall, did not occur in this simulation. However, the phosphate backbone directly attached itself to the inner walls of the nanotube with no intervention by water molecules leading to an increase in the intra-strand separation between phosphate atoms. It has to be kept in mind that the only structure that is viable for conformational changes is the furanose ring which connects the bases with the phosphate backbone. Therefore, the bending away of the DNA bases from the closest nanotube wall is brought about by the conformational changes of the pentagonal sugar ring. The insertion of electrically stretched DNA into CNT was experimentally demonstrated by Okada and coworkers [42] via electrophoresis.

MD simulations reveal that spontaneous conformational change of the DNA bases enables them to self-assemble with the CNT surface through π–π stacking (Sec. 2.3). The nucleobases undergo a conformational rotation of 90° relative to the sugar phosphate backbone, so that they get detached from their neighboring bases before stacking on the nanotube surface. The other nucleobases diffuse towards the nanotube from axial and radial directions as a result of which the phosphate backbone draws closer, facilitating adsorption of the remaining nucleobases to the sidewalls [34]. Desorbed bases are stabilized by stacking interactions within adjacent bases. Electrostatic and torsional interaction within the phosphate backbone leads to helical wrapping of DNA around the CNT. Simulation shows that torsion and helical wrapping is generated from the 3'-end of the strand and consequently propagates towards the 5'-end. Even the DNA strands associate with the CNTs in several configurations, including loops and kinked structures [15]. As predicted by simulation studies, there is a high preference for loop formation which is indicative of the maximization of CNT base stacking by minimizing the free energy of the hybrid system. This phenomenon of looping is independent of DNA sequence. It has been predicted by MD and proved experimentally [33, 43] that orientation of the bases depends only on their identity and not on the diameter and chirality of the CNT [32]. It has been observed that bases, depending on their identity, have a definite orientation relative to the tube axis (Sec. 5.6). This is due to the van der Waals interaction between the bases and the CNT curved walls which maximizes the spatial interaction between them.

Studies of the absorption of adenine and thymine molecule on CNT revealed that there was no significant deformation on the nanotube surface or on the molecules upon adsorption. The electronic structure of both metallic and semiconducting nanotubes was not changed significantly due to this physisorption, which results in only small modifications in the electronic properties of the CNT [35]. The presence of the Pauli barrier [31] between the π orbitals of the molecules and the π orbitals of the nanotubes results in the minimization on π–π interaction between the two and also determines their equilibrium distance of separation. In spite of the repulsive forces between the π orbitals, immobilization of DNA bases on the surface of the CNT is largely attributable to the attractive exchange-correlation interaction, which dominates over the Pauli repulsive forces. All the nucleobases experience π–π stacking interactions with the nanotube, with stacking energies and binding energies [44] dependent on the number of aromatic rings of the base and also the surface area of interaction. Due to its largest surface area amongst the DNA nucleobases, guanine experiences the strongest van der Waals attraction with the nanotube. The total binding free energy of the DNA-CNT hybrid is not the sum of binding energies of the CNT and of the individual bases, but depends on the sequence of the DNA. Calculation of the density of states (DOS) showed small charge transfer from the radicals of the bases of DNA to the nanotube, because the charge redistribution was preferentially limited to the radical as compared to the molecule. An understanding of the interaction of individual bases (adenine and thymine) with the nanotube encouraged the researchers to model DNA-nanotube electronic interactions. Lu and coworkers [45] simulated the electronic interaction between an infinitely long DNA molecule with a periodic array of the CNT, and computed the DOS of the combined system. It was also observed that in an aqueous environment, the base pairs tend to twist and bind to the CNT surface, mediated by electrostatic potentials between them. The band gap (E_g) of the combined system of (10, 0) semiconducting CNT and dry neutral DNA is found out to be 1.7 eV, which is lower than that of DNA ($E_g = 2$ eV) but higher than that of (10, 0) CNT ($E_g = 1.4$ eV), attributed to the presence of unoccupied states of the CNT that fall within the band gap of DNA. It was also showed that due to the states being generated through hybridization of atomic orbitals, the CNT shows metallic behavior, and transport through DNA occurs by electron hopping.

Martin and coworkers [46] used all-atom exchange MD simulations to study the association of several ssDNA sequences (i.e., the homo-oligomers d(T) (TTTTTTTTT) and d(G) (GGGGGGGGGG); and the hetero-oligomer d(TG) (TGTGTGTGTG)) with CNT of different chiralities (i.e., a (6, 5) tube with diameter of 7.46 Å, and a (15, 2) nanotube with a diameter of 12.6 Å) in aqueous medium. Computation was carried out using the GROningen MAchine for Chemical Simulations (GROMACS) [47] simulation package. The potentials for DNA and counter-ions were derived from the optimized potential for liquid simulations-all atoms (OPLSAA)-2001 force field and the transferable intermolecular potential-3 point (TIP3P) model. To reveal the binding of DNA to the CNT surface, the researchers studied the variation of centre of mass (COM) between the oligonucleotides and the nanotube axis, with time expressed on the scale of picoseconds. The decrease in the COM is attributed to the association of the oligonucleotides with the CNT. It has been observed that within 1000 ps, there is a rapid drop in COM, confirming fast partial absorption of DNA on the CNT, followed by slow structural reorientation to form a bound state, suggesting that sequential absorption depends on hybridization kinematics. The d(G) sequence binds to the surface of the (6, 5) nanotube within 1000 ps, whereas the same binds to a nanotube of larger diameter in 2500 ps. However, the binding of the d(GT) sequence to the (6, 5) nanotube shows partial absorption as a result of a disturbed hybridization process requiring large conformational changes.

Recently, a group of researchers conducted investigations on the interaction of amphiphilic nucleosides of DNA with a

graphitic sheet [48]. Grafting of amphiphilic nucleosides on graphite has potential applications in the fields of physics, chemistry, and materials science. Amphiphiles are chemical compounds containing both polar and nonpolar functional groups, and possess both hydrophilic and lipophilic properties. MD simulations with consistent valence force field (CVFF) revealed that thymines self-assemble through polar-head to nonpolar tail joining. It was earlier predicted that because of the low adsorption energy of thymine on graphite, the presence of a sugar phosphate moiety would prevent its adsorption on a graphite surface. Confirming the earlier results, it was shown that the thymine entities that are desorbed from the graphite surface were stabilized by π-stacking and hydrogen bonding interactions. As a result, it was seen that thymine was not adsorbed flat on the CNT surface (Fig. 13), which contradicts the results reported by Mamdouh and coworkers [49]. On the other hand, the adenine molecule adheres to the CNT surface via stronger π–π interactions between them resulting in the flat absorption of adenine on the CNT surface (Fig. 14). They undergo head-to-head self-assembly (among themselves) that is stabilized by intermolecular hydrogen bonds. These amphiphilic self-assembled nanostructures physisorbed on graphite have been seen experimentally through high resolution STM [48].

Properties of the DFC

CNTs are long tubular nanostructures having an adequate number of delocalized π-electrons on their surface, whereas DNAs are optically active biological macromolecules, also called biological nanowires because of the abundance of π electrons (as in the case of CNTs) in which electron transport takes place by multi-step hopping. A CNT gets associated with DNA to form a hybrid system via π–π stacking interactions, as predicted by simulations and as later verified experimentally. The DNA strands bind non-covalently to the surface of the CNT through van der Waals interactions imparting fascinating properties to the hybrid system. The properties of the as-formed hybrid material depend not only on the sequence of nucleosides on the strand but also on the relative abundance of certain bases (Sec. 4.4). Here, we present a brief and focused discussion on the most intriguing properties of DFC.

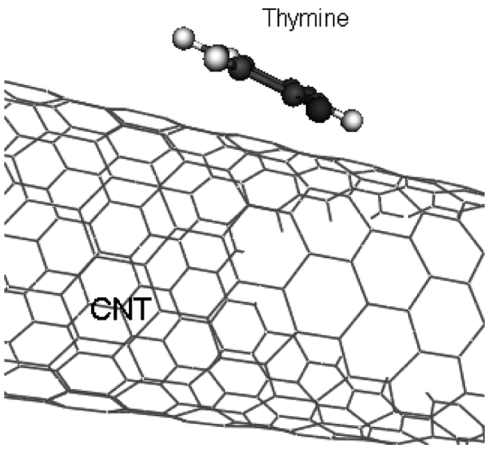

FIGURE 13.—Stable configuration of thymine showing that it is not adsorbed flat on the CNT surface.

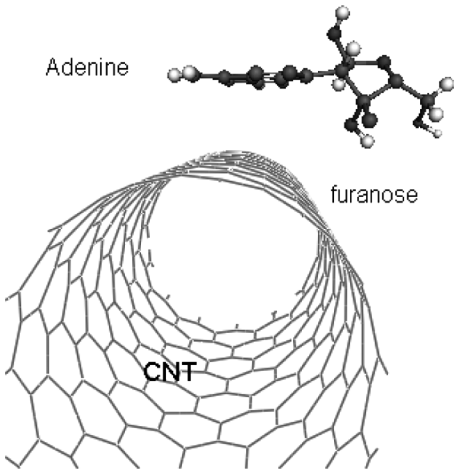

FIGURE 14.—Stable configuration of adenine showing flat adsorption on the CNT surface.

Electrochemical Properties

CNTs have lured researchers in the search of possible applications in electrochemical sensing and detection because of properties, such as their high surface-to-volume ratio, fast heterogeneous charge transfer, and electrochemical stability. DFC has the ability to be used as novel, label-free, and sensitive sequence-specific detectors of DNA through an electrochemical approach. Zhu and coworkers [50] and Zhou and coworkers [51] reported dramatic increase in electron-transfer resistance of the electrode surface upon DNA immobilization. The voltammetric response of CNT-DNA composites depends on the wt% of DNA used to functionalize the CNTs [52]. The investigators reported that with 0.5 wt% DNA voltammograms exhibited maximum current responses, attributable to the best dispersion of CNT at this wt% DNA. It was also asserted that MWNT and SWNT showed similar electrochemical responses, making MWNT suitable for use in detection devices. Hu and coworkers [13] devised a technique for electrochemical detection of low concentrations of dopamine using ssDNA functionalized CNTs. They conducted experiments to study the efficiency and applicability of DFCs for electrochemical detection and to determine voltammogram responses at low concentrations. ssDNA functionalized SWNT were deposited on glass in the form of a film fabricated into working electrodes. The latter showed flat and wide potential window under cyclic voltammogram analysis with no redox reaction in the potential window, implying high signal-to-noise ratio for electrochemical detection. The investigators used $Fe(CN)_6^{4-}/Fe(CN)_6^{3-}$ redox pairs for their voltammogram analysis, which were found reproducible in all but the first cycle, since the distribution of oxidative/reductive reactant in the starting concentration near the electrodes was different from that in later cycles. It was also observed that the diffusion speed of redox pairs

across the electrodes determined the speed of the reaction, and that the electron transfer speed between the interface of the electrode and the solution was faster than the diffusion of redox pairs, as a result of which the reaction was termed quasi-reversible. Since the voltammograms are reproducible without any chemical pretreatment, it can be concluded that the surface of the electrode is deactivated unlike that of other carbon-based electrodes.

The electrochemical behavior of immobilized calf thymus DNA molecules on the surface of MWNT was also studied by cyclic voltammetry (CV) and electrochemical impedance analysis (EIA) [53]. First, the electrochemical behavior of the gold-modified MWNT electrode was studied through CV, showing a couple of redox peaks that become stable after subsequent cycles, and revealing that the MWNT contains carboxylic acid groups that aid immobilization of DNA. The process of immobilization was brought about by compounds 1-ethyl-3-(3-dimethylaminopropyl) carbodiimide hydrochloride (EDC) and N-hydroxy-succinimide (NHS), which help the formation of amide bonds between the carboxylic group of the MWNT and the amino group of the DNA bases. When the DNA has been immobilized on the surface of the MWNT, the redox peaks of –COOH vanish and background current decreases due to DNA coupling to the MWNT electrode. The authors also observed that the redox peak current decreases with increase in immobilization time. This relationship can be attributed to the low conductivity of DNA molecules, resulting from insufficient electron transfer between the redox probe and the electrode surface, in turn resulting from the interaction between carboxylic groups of the MWNT and the amino groups of the DNA. Saturation of DNA on MWNT takes about 3 hrs and can be observed from the decrease of the anodic peak current of the redox probe up to 3 hrs, after which it does not show a substantial decrease. EIA, obtained by Nyquist plots, reveal that CNT modified electrode has high conductivity and that the redox behavior is a diffusion-controlled process [Fig. 15(a)]. On treating the MWNT-modified electrode with DNA, aided by EDC/NHS for sufficiently long time until saturation occurs, the Nyquist plot shows a semicircle [Fig. 15(b)], which can be attributed to the inhibition of the redox process resulting from the immobilization of DNA on the surface of the MWNT. The

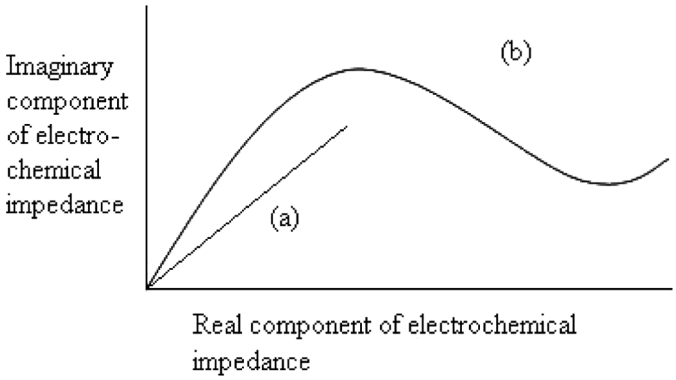

FIGURE 15.—Typical diagram of a Nyquist plot. Electrode modified with (a) untreated CNT and (b) DFC.

–COOH groups are often introduced on the walls and end-caps of the CNT during purification. The carboxylic groups aid the immobilization of DNA by covalent interactions. Small electron-transfer resistance implies that amount of DNA adsorbed to the surface of the MWNT is small, and that the covalent bond between the amino groups of DNA and the –COOH groups of MWNT predominate. The problem was solved by washing with phosphate buffer, thus minimizing the stray signals due to DNA immobilization [54]. It has been reported that a well-aligned CNT array and high reactivity of the CNT caps facilitate high reactivity and stability of grafted entities on CNT, as required for advanced electrochemical devices. Efforts have been made for more sensitive electrochemical detection of DNA hybridization based on electro-polymerization of DNA on MWNT paste electrodes and for examining the current response through ethidium bromide, an electroactive intercalator [55].

Chemical Properties

The CNT-DNA hybrids exhibit photo-catalytic properties that induce photo-reduction of Ag^{+} to Ag^{0}, whereupon the charge-transfer band gives the signature of the electronic interactions between the CNT and molecular species [56]. The advantage of CNT-DNA catalysts lies in better control and characterization of the reaction mechanism. Wrapping of DNA over CNT provides for variable binding sites on the substrate. Dai in his review [57] stated that due to the presence of hydroxyl and phosphate functional group in DFC can be used for chemisorption of certain chemical species. Again, the non-covalent bonding of DNA with CNT via π-stacking of base pairs, imparts thermal stability to the functionalized hybrid.

Napier and coworkers [58] studied the electro-catalytic oxidation of DNA wrapped CNT by tris (bipyridine) ruthenium(II) ($Ru(bpy)_3^{2+}$) at indium tin oxide electrodes in neutral solution. Experiments conducted by the authors showed that since $d(T)_{60}$ oligonucleotide contains no oxidisable guanine, there is no current enhancement in the sample that contains $Ru(bpy)_3^{2+}$ compared to the sample containing $Fe(dmb)_3^{2+}$. However, addition of $d(T)_{60}$ wrapped CNT produces a significant increase in current. This is attributed to the oxidation of CNT by Ru^{3+}, generated electrochemically. On the other hand, there was no increase in current for $d(T)_{60}$ wrapped CNT in Fe $(dmb)_3^{2+}$, which conveys that the rate of electron transfer is greatly reduced at lower potential. However, at higher concentrations of CNT, catalytic current could be detected for $Fe(dmb)_3^{2+}$. The presence of DNA lessens the quantity of CNT required to produce a signal.

Electrical and Electronic Properties

The behavior of the DNA-CNT hybrid system gets greatly modified by the nature of the CNT chosen, i.e., metallic or semiconducting, as they have a dissimilar band structure with different energy levels. Functionalization of nanotubes with DNA provides an elegant method for separating semiconducting nanotubes from metallic ones. Semiconducting to metallic transitions, triggered by water molecules, have also been observed in DFC.

Hembram and coworkers [59] conducted electrical conductivity studies (impedance spectrum analysis, and DC and AC conductivity) on CNT-DNA composites and found that conductivity of composite increases with increase in CNT concentration. The impedance spectrum of DFC was characterized by a semicircular arc whose intercept on the real axis provided information about the electrical behavior of the hybrid. The decrease in the radius of the semicircular arc signifies as decrease in resistance or an increase in conductivity. It was revealed [60] using a Nyquist plot (Sec. 4.1) conducted on DFC-modified Pt electrodes for measurement of electrochemical impedance, that apart from the semicircular part, the plot also contains a linear portion. The semicircular part that appeared at higher frequencies corresponds to an electron-transfer limited process, and the linear portion, appearing at lower frequencies, is attributable to a diffusion process. Recently, Basuray and coworkers [61] devised an open-flow impedance sensing platform to detect DNA hybridization of CNT produced by high frequency AC electric fields. The arrangement minimizes double layer formation near the CNT interface, thus facilitating easy detection of impedance signals.

Chou and coworkers [10] used the photoluminescence (PL) (Sec. 5.5) and resonant Raman spectroscopy (RRS) (Sec. 5.6) techniques to study the electronic properties of semiconducting CNT through a process of DNA-wrapping and ion-exchange chromatography (IEC) fractionalization. The DNA wrapping isolates individual CNTs and the IEC fractionalization separates the metallic nanotubes. They concluded that DNA wraps selectively on CNTs. This selectivity was used by Zhang and coworkers [62] for chirality-based separation of (10, 5) CNT by the ion exchange method. With the use of a 13-mer DNA sequence of $(TTTA)_3T$, they achieved 99% richness of single chirality (10, 5) nanotubes, which due to their larger diameter were most suitable for FET-based applications. Earlier, the same group achieved 94% richness of (7, 6) and (8, 4) nanotubes using $d(GT)_{20}$-DNA [63]. It has been emphasized that fragment length and sequence composition, especially the GC content plays a vital role in selectivity of CNT [64]. UV measurement and photoluminescence excitation (PLE) analysis also generated sufficient information about the modification in the band structure of DNA-CNT hybrid material (Secs. 5.4 and 5.5).

Recently, Cha and coworkers [65] detected reversible metallic to semiconducting transitions in nanotubes when SWNTs were wrapped with ssDNA. The researchers concluded that the water molecules played a dominant role in producing this transition, as the interactions between water and DNA often modify the behavior of the system. This metallic to semiconducting transition was measured by FET, the electrodes of which were fabricated by nanoimprint lithography (NIL) to obtain a precise 300 nm gap between electrodes (source and drain). Predominantly metallic nanotubes were deposited in between the electrodes by dielectrophoretic deposition. Dried and non-functionalized SWNT showed no change in source-drain current. Even dried and ssDNA functionalized SWNT revealed no significant change in conductivity. The source-drain current showed sharp contrast when ssDNA functionalized SWNTs were hydrated, resembling *p*-type semiconductors with a threshold voltage occurring at about -7 V. The results were found to be reproducible under both hydrated and dehydrated conditions. It was noticed that the current responses were nearly zero in the range of the positive gate voltage when hydrated DFCs were tested, which confirms that the majority of the DNA functionalized metallic nanotubes made transitions to the semiconducting ones only as a result of hydration. DNA sequence does not play a significant role in such transitions.

Dispersion and Solubility of DFC in Water

CNTs are hydrophobic nanotubes that exhibit poor solubility in water because of their clustered state. But with the introduction of DNA in the medium under sonication, interaction of DNA with CNT occurs leading to wrapping of CNT by DNA, which isolates individual nanotubes, thereby leading to sufficient dispersion. However, it is reported that pyrenyl group (containing large aromatic rings) modified DNA does not effectively wrap the SWNTs of larger diameter as a result of which stable dispersion cannot be achieved [66]. It was observed by Li and coworkers [52] that 0.5 wt% DNA-functionalized MWNTs exhibit a solubility of 1 mg/ml. The suspension of functionalized MWNTs was reported to be stable for several months. The high solubility of DFC is attributed to the negative charge on the phosphate backbone of the DNA, whose nitrogenous bases are non-covalently attached to the surface of the CNT via $\pi-\pi$ interactions. Similar non-covalent carboxylic functionalization of SWNT has also been reported [67]. Solubility of CNT upon DNA wrapping also depends on the abundance of bases, in the order C > T > A > G in the DNA sequence. It was experimentally seen that CNTs were most efficiently dispersed when the DNA sequence was rich in cytosine, and that richness of guanine would lead to unsatisfactory debundling of CNT [33].

DNA has proved to be the most suitable material for stabilizing the CNT in water. At the same time DNA forms a homogeneous suspension of chemically unmodified nanotubes in water. Badaire and coworkers [68] constructed a phase diagram (-nanotube concentration vs. denatured-DNA concentration) to study the efficiency of DNA as stabilizing agent for CNT for sufficiently high concentration of either constituent. The phase diagram shows two regimes separated by a line passing through the origin. The phase above this line shows that the nanotubes are well dispersed on sonication for a considerable time. The phase below this line depicts that at low DNA concentration, nanotubes aggregates were found, even after sufficient sonication, because of inadequate wrapping of DNA over the CNTs. The thermodynamic behavior between the dispersed and the aggregated phases of the nanotubes, seen with separation between their domains, helps to achieve a higher concentration of the nanotubes just by mere evaporation of the solvent. It was observed that for nanotube concentration in the range 2–4%, the nematic and isotropic phases coexist in the medium, as is evident from optical micrographs that clearly showed birefringent domains separated from each other. These birefringent domains were found to coalesce when the neighboring domains touched each other. With further

drying, when the nanotube concentration exceeds 4%, the system forms a water-based nematic phase of freely suspended, non-functionalized nanotubes, depicted by the classical Schlieren texture of the nematic phase.

Optical Properties

Optical properties of materials are the outcome of their electronic band structures. Optical measurements aim to explore the signature electronic transitions that are occurring within the substance, with or without external excitation. DFCs show anisotropic response to both linearly and circularly polarized light. Optical methods have been utilized to study the electronic energy level modification upon DNA hybridization. An optical probe to the hybrid structure provides information on the orientation of DNA bases on the surface of CNTs, and also on the nature of interactions between the DNA and the CNTs.

Hazani and coworkers [69] covalently modified SWNTs with DNA via carbodiimide-assisted amidation, yielding a highly water-soluble adduct. The interactions between the SWNT and DNA were examined by UV-vis spectroscopy and confocal fluorescence microscopy. The former characterization revealed that the majority of the DNA present in the adduct was covalently bonded, rather than simply physisorbed. Later characterization images, apart from confirming the earlier results, showed micron-size features that were a direct consequence of the aqueous solubility of the DNA-functionalized SWNTs.

Meng and coworkers [32] reported a preferred absorption direction for the bases on the CNT. The intrinsic and diameter-dependent absorption peaks of CNTs occur between 200–260 nm. Since the phosphate group and the sugar do not make significant contribution to the optical absorption of DNA, any modification in optical absorption of CNT after DNA functionalization can be attributable to the preferred absorption direction of the bases on the surface of the CNT. These changes in absorption spectrum for the CNT-DNA system are also observed in the same range of the spectrum. Upon UV irradiation, since CNT absorption in the perpendicular direction is much larger than absorption in the parallel direction, the availability of photons with polarization parallel to the CNT axis is greater than that of photons with polarization perpendicular to it. In other words, nanotube produces a local electric field aligned along the axis of the nanotube, facilitating the interaction of DNA bases with the CNT. The screening effect of this polarization by bound DNA, and the averaging effect of the local field around the CNT-DNA system by the thermal fluctuation of counter-ions and water, will result in more absorption by the base in the direction parallel to the tube axis than perpendicular to it. This effect is called hypochroism of DNA and provides the reason behind the change in absorption spectra of DNA bases when they are attached to nanotubes in the direction of the nanotube-axis. Using this principle, the orientation of bases relative to the CNT axis in the DNA-CNT system was explored. Hughes and coworkers [33] studied the interaction of CNT with DNA and concluded, through UV-optical absorption measurements, that DNA binds to nanotubes through π-stacking. They also observed anisotropic hypochromicity of optical transitions in DNA bases hybridized with SWNTs. The inherent chirality of DNA makes it optically active. This leads to anisotropic absorption for left and right circularly polarized light leading to a phenomenon called induced circular dichroism (ICD) (Sec. 5.6) This phenomenon of induced circular dichroism results from coupling between transition dipole moments of optically active electronic transitions in chiral molecules, and transition dipole moments of nearby interacting molecules that may not be necessarily chiral. The coupling, having contributions also from the magnetic transition dipole moments [70], occurs between transition dipole moments of optically active and chiral DNA macromolecule, and the transition dipole of non-chiral CNTs. It was observed that as nanotube transition energy increases and approaches the DNA transition energy there is an increase in CD intensity, as predicted by the theory of ICD. Using the principle of ICD, investigators [71] have devised techniques to detect traces of chemicals that can disturb the coupling effect of the transition dipole moment between DNA and the CNT. They have found that Hg^{2+} ions have strong binding affinity towards bases of DNA that are bound to the nanotubes, as a result of which the interaction between the CNT and DNA becomes weaker as the strands loosen from the CNT surface. To find the effect of DNA sequence and length on the dispersion efficiency of DNA, Zheng and coworkers [14], through optical absorption measurements, concluded that 30-mer poly (T) shows the highest yield.

Apart from the properties of DFCs discussed above, the vibrational properties of DFCs need mention. A recent technique called surface enhanced IR absorption (SEIRA) has been adopted to study the interactions between DNA and CNTs [72] that produce changes in the vibrational modes of DNA. A strong interaction between DNA and CNTs was observed as indicated by changes in the DNA marker bands as a shift of the phosphate I band in the high frequency region, and as a low frequency shift in the phosphate II band. Moreover, the SEIRA spectrum revealed transformation of H-bonds in the region of –OH, –NH, and –CH vibrations as a result of attachment. On the basis of increased intensity of vibrations in the region of 600–900 cm^{-1}, the authors claimed that the nucleic acid molecule wraps around the CNT, though it has not been confirmed by micrographs.

Characterization techniques for DFC

SEM

High-energy focused electron beam, incident on the surface of a sample may generate primary electrons, secondary electrons, X-rays, back-scattered electrons, and auger electrons from the surface, through the process of elastic and inelastic scattering. As the electron probe rasters across the sample surface two-dimensionally, the signal in the form of secondary electrons, generated from the surface, can be detected, amplified, and displayed on the CRT screen as brightness-controlled and magnified images. This is the basic principle behind the working of SEM.

Li and coworkers [52] showed that when the wt% of MWNT exceeds 2% than that of the DNA solution in ultrapure water, agglomeration of MWNT takes place leading to insufficient dispersion. Below 2 wt% of MWNT,

the SEM micrograph shows thick and dense covering of DNA strands on MWNT attributed to the π–π interaction between the DNA and the MWNT, leading to high binding affinity between them. It was also seen that due to the presence of excess DNA, the MWNTs could be entirely wrapped by DNA.

STM

STM is based on the phenomenon of quantum-mechanical electron tunneling through a finite barrier. Each atom has an electron cloud around it, and when the STM tip is brought near the specimen surface, the electrons can quantum mechanically tunnel across the gap, causing a current to flow called the tunneling current, which is responsible for the generation of the STM image. The tunneling current falls off exponentially with distance between the tip and the surface, and if the tip and the sample are scanned using piezoelectric drivers, the STM image reflects the variation in sample surface topography. STM can only be used for conductive specimens; so biological specimens have to be stained with heavy metal before imaging, resulting in a loss in spatial resolution.

Several morphological details of the DNA-CNT hybrid or DFC can be obtained from the STM studies. It predicts a wrapping pitch of DNA around CNT to be 3.3 nm which is in close agreement with MD simulation investigations with (6, 5) nanotubes. Yarotski and coworkers [73] conducted STM measurements at low temperature and in ultrahigh vacuum using a 20-mer DNA-CNT hybrid deposited on *p*-doped Si-substrate. The regions of DNA wrapped around a portion of the CNT can be observed as island-like protrusions on the flat substrate surface depicting regular height modulation of the DNA. Depth monitoring in the longitudinal direction to the CNT axis gives the coiling pitch of the DNA. It also gives the modulation depth of 1–2 Å, which is attributed to the thickness of the phosphate backbone coiling over the CNT. Peaks and dips in the topographic image represent the DNA strand and the CNT surface, respectively. The Fourier transform of a wrapping section in longitudinal coordinates depicts the spatial distribution of peaks in a given section spanning over the entire length of the DNA wrapped CNT. Depth monitoring in the direction transverse to the CNT axis reveals that the wrapped section of the DNA makes an angle of 63.4° with the CNT axis for a DNA sequence of $5'NH_2$(C-6)GAGAAGAGAGCAGAAGGAGA-3′. Though not discussed in detail, the investigators claimed that this angle heavily depends on the DNA sequence and on the chirality of the CNT. Thus, STM measurements can preferentially distinguish between DNAs of different sequences wrapped around a CNT of known chirality. It has also been reported that periodic modulations along the DNA length have two characteristic lengths, 1.9 and 2.5 nm.

AFM

STM uses the current flowing between the specimen and the probe tip to construct the topological image of the surface. An AFM uses the van der Waals forces between the tip and the sample to form an image of the surface topography. The record of vertical motion of the tip is reflected through the deflections in a laser beam, detected by a position-sensitive detector (PSD). AFM can be used in contact, non-contact, and intermittent modes for the construction of images of surfaces.

AFM has been effectively used to image DNA-wrapped CNT dispersed over a mica substrate [74]. The length of the ssDNA, its wrapping pitch, and the number of turns it makes over the CNT has been calculated using simple mathematical relations. In the AFM image, the wrapping of DNA over CNT has been depicted by peaks and valleys, showing the surface pattern. The difference between adjacent peaks gives the pitch of wrapping of DNA over the CNT. It has been asserted by MD simulations that wrapping pitch of greater than 10 nm is unfavorable [34] but later verified by AFM imaging to be 3.3 nm. AFM could also detect the length (number of oligonucleotide) of the DNA, as pitch and peak widths are higher for larger DNAs. However, the DNA sequence could not be sensed.

DNA sequencing with AFM using a CNT probe has been reported by Burns [75]. A CNT probe functionalized with individual DNA nucleotide experiences different forces when brought in close proximity to complementary DNA nucleotides, like thymine and adenine or cytosine and guanine, which can be readily detected and produce measurable deflections on the cantilever. Burns and his coworkers used thymine functionalized force probe to scan ssDNA grafted on mica and measure the positions of the complementary bases. They extended their work by developing functionalized CNT probes for DNA sequencing [76]. They performed their experiments on 20 nm long ssDNA with 60 nucleotides. A thymine functionalized CNT hunts for its complementary base, i.e., adenine, while scanned across the length of DNA, and experiences a phase lag in the location of adenine molecules when the atomic force microscope is operated in tapping mode. The phase lag in AFM has been depicted as a darker region on the ssDNA and is a result of the interaction between the thymine and adenine molecules. It is to be noted that the diameter of the CNT probe must be less than the distance between the complementary bases of DNA to yield better spatial resolution of the target ssDNA. Researchers are working on functionalizing the CNT probes with multiple nucleotides, so that the same probe can be scanned across the entire ssDNA.

Gigliotti and coworkers [77] conducted experiments with genomic DNA and asserted through AFM analysis that ssDNA had the ability to wrap tightly around CNT forming close and compact helices of uniform pitch. They also asserted that wrapping of DNA around the CNT was not a sequence-dependent process, as they employed genomic DNA that was completely random in sequence. Zheng and coworkers [14] conducted AFM measurements which showed that CNT diameters are slightly higher (1–2 nm) than the typical HiPCO nanotubes (0.7–1.1 nm), but showed DNA wrapping.

Buzaneva and coworkers [78] characterized the DNA wrapped CNTs using AFM that showed networks with pronounced structures of DFC. AFM images of ssDNA–SWNTs and ssDNA–MWNTs indicated that no self-aggregation was caused by the attachment of DNA chains [8].

UV-Visible Absorption Spectroscopy

UV light, on its passage through the sample solution, is absorbed to a certain extent. Thus the intensity of the transmitted light (Say I) is always less than the intensity of the incident light (Say I_0). According to the Beer–Lambert principle, transmittance (T) is given by the relation

$$T = \left(\frac{I}{I_0}\right) e^{-\varepsilon l c}. \quad (1)$$

Absorbance (A) is expressed in terms of transmittance (T) by the relation

$$A = -\log_{10}(T), \quad (2)$$

where ε is the molar extinction coefficient, c is the concentration of sample in the solution, and λ is the path length of incident UV-visible (UV-vis) radiation through the sample. The molar extinction coefficient (ε) is a function of the wavelength of radiation which makes absorption also a wavelength dependent process. The nature and the position of the absorption maxima that occur at a wavelength λ_{max} depends on the size of solute particles and relative orientation of hybrid structures dissolved in the solution. The spectrum obtained from the UV-vis spectrophotometer is called the UV-vis spectrograph. UV-vis spectrophotometers are equipped with spectral bandwidth ranging from 200 nm to 1100 nm that covers a portion of the UV region (<380 nm), the visible region (380–760 nm), and a portion the infrared region (>760nm). Thus UV-vis spectrograph can provide information not only in the ultraviolet region, but in the visible and infrared regions too, as detailed below.

Hughes and coworkers [33] provided early experimental evidence of π-stacking of DNA bases with SWNT through UV measurements. The investigation was carried out by analyzing the anisotropic hypochromic absorbance, which is a characteristic of π-stacked structures, in which the variation in absorbance of free and bound states of DNA is attributed to the DNA dipole transitions that lie along the axis of the optically anisotropic CNT, governed by the preferred orientation of the nucleoside bases with respect to the nanotube long axis. Hazani and coworkers [69] studied the UV-absorption of the interaction between amino-modified SWNT and DNA, and concluded that DNA is not physisorbed on the modified nanotubes, but is held together by covalent bonds between amino-group and bases of DNA. The researchers asserted that the absorption peak at 265 nm found from the UV-vis spectrograph was caused by the absorption maximum of DNA, as absorption peaks for CNT are too weak to be observed because of background light scattering. But Huang and coworkers [79] argued that strong peak around 270 nm also has contributions from impurities present in the sample. They conducted experiments which showed that the dominant peak intensity around 270 nm dramatically decreases upon performance of size exclusion chromatography (SEC), which cuts off impurities according to their sizes. With ion exchange chromatography (IEC), the intensity of the 270 nm peak further decreases, and the base line is in the lowest position, which exposes finer, smaller peaks in the neighborhood of 270 nm. They further clarified that since pure ssDNA gives an absorption peak at around 260 nm, the small peaks of DNA wrapped CNT around 270 nm were subdued within the strong 270 nm absorption peak due to the presence of carbonaceous impurities.

UV-vis absorption spectroscopy plays an effective role in the recording of electronic transitions between the van Hove singularities of both metallic E_{ii}^M and semiconducting nanotubes E_{ii}^S [80]. The peaks in the UV-vis spectrograph, centered in the range 440–600 nm, are assigned to the first van Hove singularity of metallic SWNT (E_{11}^M) and peak centered in the range of 600–800 nm to the second van Hove singularity of the semiconducting SWNT (E_{22}^S). It is obvious from the results that the electronic properties of the pristine SWNT are conserved even after the formation of a DNA-CNT hybrid. It was reported that DNA-functionalized MWNT yields characteristically dull absorption peaks at around 774, 895, and 1019 nm that are attributable to the semiconducting band of the MWNT [81] along with a peak at 260 nm as the characteristic peak of ssDNA. Since the metallic CNTs have absorption peaks in the range 400–600 nm, UV-vis measurements provide a good amount of information about metallic CNT, which is not obtained by PLE measurements. But for the analysis of semiconducting CNT, Zhang and coworkers [63] insisted that PLE data can distinguish among CNTs of similar diameter but of different chiralities that contributes to the same first subband absorption peak in UV measurement data.

UV-measurements have also revealed that richness of cytosine and deficiency of guanine bases in DNA sequences aids in better dispersion of CNTs (Sec. 4.4). CNT samples dispersed by wrapping of cytosine rich DNA showed well-resolved absorption peaks of isolated individual CNTs against dull and featureless absorption peaks of samples dispersed by guanine-rich DNA [33].

PL Investigations

Fluorescence and phosphorescence refer to physical phenomena in which the system absorbs a particular wavelength of light and emits light at a higher wavelength that depends on the electronic structure of the system. When the system is excited by UV-vis radiation, the electrons residing in the ground state jump to the higher energy level and, consequently, fall to a lower vibrational state within the same electronic level via non-radiative transitions. When the lifetime of electrons in this metastable state is of the order of 10^{-8} sec, following which they return to the ground state through radiative transitions, the phenomenon is termed as fluorescence. The phenomenon of phosphorescence occurs when the electrons stay in the metastable state for 10^{-3} sec or more, due to forbidden pathways, before falling to the ground state via radiative transitions.

IEC is widely used for the diameter-assisted separation of nanotubes in distinct and eluted fractions. These eluted fractions were studied for CNT fluorescence by Strano and coworkers [82]. It has been established that a DFC experiences a red shift in its PL and Raman spectra as compared to sodium dodecyl sulfate (SDS)-encapsulated

CNT. Here the authors argue that no such shift was observed in their experiments, further suggesting that the red shift was likely due to incomplete coverage of oligonucleotide strands of DNA on the surface of the CNT, thus allowing water molecules to penetrate in between the wrapped DNA layer and the CNT and thereby interact with the CNT directly, modifying the electronic behavior of the system.

PL measurements were conducted over a wide range of excitation energies by Chou and coworkers [10] to investigate the effects of fractionalization and DNA wrapping on CNT. The E_{11}^S and E_{22}^S transitions for non-fractionalized specimens of DFCs in the near IR region were determined by a contour plot of excitation energy vs. emission energy, both expressed in electron volt (eV). The excitation and energy peaks have been observed for both fractionalized and non-fractionalized DNA-CNT hybrids and correlated with E_{11}^S and E_{22}^S energies obtained for SDS-encapsulated HiPCO nanotubes in another work by Strano [83]. He reported that PL energies showed a red shift of less than 30 meV in E_{ii} energies for DFC as compared to SDS-encapsulated nanotubes; this red-shift was attributed to different perturbation of nanotubes with different wrapping agents and varied chemical environments. The fractionalized and non-fractionalized samples show differences in E_{ii} energies signifying that though DNA-wrapping isolates individual nanotubes by increasing the inter-tube distance, the degree of homogeneity in the nanotube environment induces a change in the electronic structure of the individual CNT because of interactions with different species. Fractionalization of DFC eliminates other brighter luminescent species and brings out weaker transitions occurring within the given species that were in the original sample. This was confirmed by the absence of (9, 7) and (10, 0) SWNT peaks in the PL spectra of non-fractionalized samples, but it is present in the PL contour plot of the fractionalized counterpart.

Raman Spectroscopy

When a polychromatic incident beam is allowed to fall on a transparent substance, a small portion of the light is scattered with altered frequency. A vibrational transition is triggered in the system when a photon of frequency ν_{inc} is absorbed and a photon with frequency ν_{emit} is emitted. The scattering of emitted photons gives rise to two observed cases—one with $\nu_{\text{emit}} > \nu_{\text{inc}}$ corresponds to an anti-stokes line, and the other with $\nu_{\text{emit}} < \nu_{\text{inc}}$ called the stokes line. This phenomenon, termed as Raman scattering, determines the vibrational energy levels of a system.

Zheng and coworkers [14] carried out a series of Raman analysis of different eluted fractions of samples obtained from IEC in an effort to separate the metallic nanotubes from the semiconducting ones. IEC is a process that facilitates the separation of ions and polar molecules based on coulombic interaction between charged molecules. Fraction 47 (f47) shows stronger absorption in the metallic E_{11}^M band (400–600 nm) and weaker absorption in the semiconducting E_{11}^S band (900–1600 nm) than fraction 49 (f49) of the DFC, signifying that the earlier eluted fraction is predominantly made up of metallic nanotubes. These results have been confirmed by the observation of the strongest Breit–Wigner–Fano line-shape component in the tangential *G* band near 1,600 cm^{-1}, which is associated with metallic nanotubes. Further, the electronic spectrum of f49 was 5 nm red-shifted relative to that of the f47, as reported.

Under Raman analysis, DNA wrapped MWNT shows a red-shift of about 8 cm^{-1} at 1580 cm^{-1} due to electronic charge transfer between DNA and the walls of the CNT [52]. In the process of purification by acid treatment, some –COOH functional groups are attached to the walls of the CNT. In the DNA-CNT hybrid, charge transfer predominantly takes place between the electron-donating amine of nucleic acid bases of DNA and the oxygen atoms attached to the CNT sidewalls. Another reason that leads to the red-shift in DFC is the induced local strain developed on the CNT due to wrapping with DNA.

The relative intensities of stokes and anti-stokes processes, carried out on DFC, show the temperature dependence of the relative phonon populations. Due to the presence of sharp van Hove singularities of the joint density of states of the hybrid systems, stokes/anti-stokes ratio is highly dominated by resonance process [10].

Radial breathing mode (RBM) of CNT corresponds to the vibration of C-atoms in the radial direction (i.e., in the direction perpendicular to the tube axis). It appears between wavenumbers 150 cm^{-1} and 300 cm^{-1}. The radial breathing mode frequency (ω_{RBM})depends on the diameter of the CNT according to the relation

$$\omega_{\text{RBM}} = \frac{C_1}{d_1} + C_2, \tag{3}$$

where C_1 and C_2 are constants, and d_1 $(=\frac{\sqrt{3}}{\pi} a_c \sqrt{n^2 + m^2 + nm})$ represents the diameter of (n, m) CNT with a_c being the C–C bond distance. Using this above expression, Strano and coworkers [82] studied the diameter distribution of CNTs. It is evident from Eq. (3) that resonance peaks in Raman spectroscopy for CNT with larger diameters are found at lower wavenumbers and that CNT with smaller diameters give Raman peaks at higher wavenumbers. When the wavelength of the excitation was 785 nm, the spectra detects the $\upsilon 2 \rightarrow c2$ transitions in semiconductors. A series of spectra of eluted samples of different diameter shows that peaks corresponding to small-diameter CNTs were absent in the latter fraction but present in the earlier eluted fractions, leading to the conclusion that small-diameter CNTs are preferentially eliminated in the earlier eluted fractions. Diameter dependence of the tangential mode has been studied through Raman spectra analysis of wavenumbers ranging from 1450–1650 cm^{-1}. Both metallic and semiconducting CNTs showed a shift in convoluted peaks from low wavenumber to larger wavenumber, corresponding to smaller to larger diameter nanotubes, respectively, with increasing elution fraction. The tangential mode in metallic CNT splits into circumferential and axial components, where the former couples with electronic states near Fermi-level to yield a Breit–Wigner–Fano line shape. The peak mode of this reflects the diameter distribution for undoped, deprotonated nanotubes that are well dispersed.

Raman spectroscopy was successfully used by Cha and coworkers [65] to detect the presence of charge carrier

dopant by shift in the G-band. It has been discussed in an earlier section that the influence of water and DNA changes the metallic behavior of dried and non-functionalized SWNT into a semiconducting one. Such metallic–semiconducting transitions were studied through close inspection of the G-band characteristics. Generally, the semiconducting SWNT is represented by a sharp and symmetric Lorentzian line, whereas the metallic SWNT is characterized by a broad and asymmetric Breit–Wigner–Fano line-shape. It was observed that dried and ssDNA functionalized SWNTs show a Fano line-shape, characteristic of metallic nanotubes. When water was introduced into the functionalized SWNT samples, transition to semiconducting state occurred, as evident from the diminishing broadness and asymmetricity of the G-band. It was further seen that the Fano peak was slightly shifted towards the higher frequency side, a characteristic of doped charge carriers.

LD and CD

LD is defined as the difference in anisotropic absorbance of parallel ($A_{\parallel}$) plane polarized light and perpendicular ($A_{\perp}$) plane polarized light by groups of molecules having varied transitional moments. Anisotropic moieties would give a nonzero LD spectrum, and molecules having a featureless LD spectrum can be thought of as isotropic association of molecules. Thus LD promises to be an effective characterization tool over UV and IR spectroscopy, AFM and TEM for the study of the orientation of respective bases on nanotubes in DFC. A positive peak in the LD spectrum signifies that the polarization is parallel to the orientation direction of molecules and a negative dip represents polarization perpendicular to the orientation direction. Rajendra and coworkers [84], with the aim of determining the orientation of the DNA molecule on a CNT with LD spectroscopy, established that DFC showed a dip in the LD spectrum at around 225 nm due to π–π^* transitions between the base and nanotube. The LD spectrum for the DFC showed a weak differential LD signal, which reveals that there was inadequate binding of DNA to nanotubes and that the bases were arranged at an oblique angle of around 54°. Though this work has shed light on the orientation between the bases and nanotubes, it lacks an explanation for the dependence of chirality of nanotubes on polarization, and the subsequent orientation of bases on chiral nanotubes. It was later shown [43] that the LD spectrum does not only have a dip at 225 nm, but also a positive peak at 275 nm. Since the LD spectrum is a contribution of all the bases with their respective orientations and a mixture of binding modes [85], the analysis remained complicated. To capture the LD spectrum below 200 nm requires a dedicated approach to minimizing the light scattering which causes loss of photons through absorbance.

CD is defined as the difference in anisotropic absorption of left-handed circularly polarized light (L-CPL) and right-handed circularly polarized light (R-CPL) while passing through the sample, and occurs when a molecule of the sample contains one or more chiral light-absorbing groups. CD is used extensively to study chiral bio-molecules for all size ranges. The CD spectrum is most helpful in the analysis of conformational changes in bio-molecules under the influence of environmental changes like pH and temperature. It can also capture the structural, kinematic, and thermodynamic interactions with other molecules. It was believed that the phenomenon of CD was not due to DNA, but to the chirality of the CNT so that the right-handed and left-handed helicities of nanotubes renders them enantiomeric to each other, exhibiting anisotropic absorption from the L-CPL and R-CPL. A CD study on the DFC was conducted by Dukovic and coworkers [86], who clarified that when a sample containing an equal number of left-handed and right-handed CNT enantiomers (racemic) was functionalized with DNA, negative and positive interaction peaks were seen in the CD spectrum, which was attributed to the DNA-induced CD (Sec. 4.5) signal being generated from the inherent chirality of the DNA.

Applications

DNA functionalized CNT hybrids find a wide cross-section of applications in nanoelectronics and sensors because of their highly reactive surfaces, rapid rates of charge transfer, and selective wrapping of DNA based on chirality of the nanotubes.

The process of DNA functionalization can separate the metallic nanotubes from semiconducting nanotubes, owing to their different electronic properties. A negative charge distribution is created on the surface of nanotubes due to the phosphate groups of the DNA-CNT hybrids that depends on the electronic property of the tube and the sequence of the functionalizing DNA. As a result of the negative charge distribution of the DNA-metallic CNT being different from that of the DNA-semiconducting CNT, the DNA-metallic CNT is predicted to have less surface charge than the DNA-semiconducting CNT, as evidenced in the opposite image charge created in the metallic tube as observed in IEC and Raman spectroscopy measurements. Again, through ion exchange methods, researchers [62] have separated out nanotubes of single chirality for FET applications (Sec. 4.3).

Lu and coworkers [9] reported preparation of 2–3 nm atomic layer, high κ dielectric film using non-covalent poly-T DNA functionalized SWNT by atomic layer deposition (ALD) technique, which enables approaching the ultimate vertical scaling limit of nanotube FETs and achieving switching of 60 mV/decade at 300 K. In the absence of DNA functionalization, severe gate leakages and shorts were observed for most of the SWNT FETs with high κ at thicknesses of less than 5 nm. But with DFCs, the leakages in gate current were reduced, leading to high performance FETs with a trans-conductance of 5000 S/m.

Applications of DFCs can also be found in the ultrafast detection of DNA hybridization [61, 87, 88], electrochemical sensing [54], polymerization of conducting polymer composites [89] and single-molecule charge transport of DNA [5].

Charge conduction in pristine CNT occurs through ballistic transport leading to high electrical conductivity of CNTs. Even after wrapping of ssDNA around the CNT, electrical measurements have shown that this non-covalent functionalization did not alter the conductivity of the individual nanotubes significantly [90]. This is due to the

presence of π-stacking interaction between the DNA and the CNT. Since π-stacking interactions are dominantly van der Waals forces, the electronic structure of pristine CNTs is preserved, as this association does not involve formation of covalent chemical bonds. Thus the researchers are interested in their possible applications as sensors [91], recognition devices [92] and in composite films where high electrical conductivity is required in addition to high mechanical strength. Here the wrapped ssDNA acts as an active chemical binding site for the chemical moieties. Single wall CNT-FET coated with nanoscale DNA can be used as chemical sensors because of their high chemical recognition capability. DFC when exposed to chemical environment, chemical species get adsorbed on the surface of the DNA, which leads to detectable variation in electronic structure and hence causes a detectable change in conductivity in the circuit. Different chemical species depending on its chemical nature will modify the conductivity of the circuit differently. Experiments showed that DFC-FET can sense, through variation in the sign and magnitude of signals, chemical species like methanol, propionic acid, trimethylamine (TMA), dinitrotoluene (DNT), and dimethyl methylphosphonate (DMMP) [91], though the mechanism of molecular detection could not be elucidated. The ssDNA increases the binding affinity of methanol thus increasing sensor response. TMA being a charged species gets adsorbed in the nanotube sidewall, through a chemical-gating effect, resulting in variation in the carrier density, in turn leading to a change in current in FET. Sensing response in propionic acid and DMMA is due to donation of protons and electrons in residual water, respectively. Experiments have shown that DNA hybridization at the contacts was the cause of the dominant sensing mechanism, as it changes the transfer characteristics because of an increase in the Schottky barrier at the contacts [93]. These experiments provided insights on the effect of binding of DNA and CNT on DNA functionality.

Conclusions

DFCs hold the exciting promise of forming the basis for new classes of chemical sensors and molecular electronic devices. DFCs are extremely sensitive to the local environment, which enables them to be used in sensor applications. But high sensitivity also causes them to be non-specific towards a particular chemical radical. DNA is associated with CNTs through $\pi-\pi$ stacking interactions, but much remains to be explored about the orientation of different bases on the CNT and the effects of DNA sequence and wrapping pitch on the properties of the functionalized hybrids. MD simulations can complement experimental investigations and can sometimes predict properties that can be exploited. MD simulations have suggested an alternative way to functionalize CNTs by inserting DNA strands inside the CNTs which was later validated experimentally. Electron transfer in ssDNA occurs through multi-step electron hopping, whereas in CNT charge flow occurs through ballistic transport. The nature of electrical transport in hybrids formed by CNT and DNA remains to be studied; it is believed that 3-D DFC network will enhance electrical and mechanical properties of composites. Since an optically active material like DNA undergoes a change in molecular optical dipole moment when exposed to certain frequencies of light stimulus, possible applications of DFCs can involve, through modulating the current in carbon nanotube field effect transistors (CNT-FETs), switching, and optical detection. To our knowledge, measurement of the optical properties of DFC on substrates has not yet been attempted; it is suspected that these properties may differ from those obtained for DFCs in solution. Efforts can also be extended to selectively separate metallic nanotubes through DNA functionalization and then utilizing them in composites for enhanced electrical behavior. Development of pH/temperature sensitive CNT bio-hybrids for repetitive use still remains a challenge for the researchers. Although much has been achieved in the field of DFCs and their possible applications, much remains to be explored.

References

1. Iijima, S. Helical microtubles of graphitic carbon. Lett. Nature **1991**, *354* 56–58.
2. Tans, S.J.; et al. Individual single-wall carbon nanotubes as quantum wires. Lett. Nature **1997**, *386*, 474–477.
3. Porath, D.; et al. Direct measurement of electrical transport through DNA molecules. Lett. Nature **2000**, *403*, 635–638.
4. Wei, D.; et al. Real-time and in situ control of the gap size of nanoelectrodes for molecular devices. Nano Lett. **2008**, *8*, 1625–1630.
5. Roy, S.; et al. Direct electrical measurements on single-molecule genomic DNA using single-walled carbon nanotubes. Nano Lett. **2008**, *8*, 26–30.
6. Mclean, R.S.; et al. Controlled two-dimensional pattern of spontaneously aligned carbon nanotubes. Nano Lett. **2006**, *6* (1), 55–60.
7. Khripin, C.Y.; Zheng, M.; Jagota, A. Deposition and meniscus alignment of DNA–CNT on a substrate. Journal of Colloid and Interface Science **2009**, *330*, 255–265.
8. Li, S.; et al. DNA-directed self-assembling of carbon nanotubes. Journal of the American Chemical Soceity **2005**, *127* (1), 14–15.
9. Lu, Y.; et al. DNA functionalization of carbon nanotubes for ultrathin atomic layer deposition of high K dielectrics for nanotube transistors with 60 mV/decade switching. J. Am. Chem. Soc. **2006**, *128* (11), 3518–3519.
10. Chou, S.G.; et al. Optical characterization of DNA-wrapped carbon nanotube hybrids. Chemical Physics Lett. **2004**, *397*, 296–301.
11. Guo, Z.J.; Sadler, P.J.; Tsang, S.C. Immobilization and visualization of DNA and proteins on carbon nanotubes. Adv. Mater. **1998**, *10* (9), 701–703.
12. Ito, Y.; Fukusaki, E. DNA as a 'Nanomaterial'. Journal of Molecular Catalysis B: Enzymatic **2004**, *28* (4–6), 155–166.
13. Hu, C.; et al. DNA functionalized single-walled carbon nanotubes for electrochemical detection. The Journal of Physical Chemistry B **2005**, *109* (43), 20072–20076.
14. Zheng, M.; et al. DNA-assisted dispersion and separation of carbon nanotubes. Nature Materials **2003**, *2* (May), 338–342.
15. Johnson, R.R.; et al. Free energy landscape of a DNA-carbon nanotube hybrid using replica exchange molecular dynamics. Nano Lett. **2009**, *9* (2), 537–541.

16. Meunier, V.; Lambin, P. Scanning tunneling microscopy and spectroscopy of topological defects in carbon nanotubes. Carbon **2000**, *38* (11), 1729–1733.
17. Zhang, J.; et al. Effect of chemical oxidation on the structure of single-walled carbon nanotubes. J. Phys. Chem. B **2003**, *107* (16), 3712–3718.
18. Park, S.; Srivastava, D.; Cho, K. Generalized chemical reactivity of curved surfaces: carbon nanotubes. Nano Lett. **2003**, *3* (9), 1273–1277.
19. Rosca, I.D.; et al. Oxidation of multiwalled carbon nanotubes by nitric acid. Carbon **2005**, *43* (15), 3124–3131.
20. Dwyer, C.; et al. DNA-functionalized single-walled carbon nanotubes. Nanotechnology **2002**, *13* (5), 601–604.
21. Baker, S.E.; et al. Covalently bonded adducts of deoxyribonucleic acid (DNA) oligonucleotides with single-wall carbon nanotubes: synthesis and hybridization. Nano Lett. **2002**, *2* (12), 413–1417.
22. Wang, Y.; Iqbal, Z.; Mitra, S. Microwave-induced rapid chemical functionalization of single-walled carbon nanotubes. Carbon **2005**, *43* (5), 1015–1020.
23. Xia, W.; et al. A highly efficient gas-phase route for the oxygen functionalization of carbon nanotubes based on nitric acid vapor. Carbon **2009**, *47* (3), 919–922.
24. Huang, S.; Dai, L. Plasma etching for purification and controlled opening of aligned carbon nanotubes. J. Phys. Chem. B **2002**, *106* (14), 3543–3545.
25. Yan, Y.H.; et al. Systematic studies of covalent functionalization of carbon nanotubes via argon plasma-assisted UV grafting. Nanotechnology **2007**, *18* (11), 115712.
26. Wildoer, J.W.G.; et al. Electronic structure of atomically resolved carbon nanotubes. Nature **1998**, *391* (6662), 59–62.
27. Jeng, E.S.; et al. Detection of DNA hybridization using the near-infrared band-gap fluorescence of single-walled carbon nanotubes. Nano Lett. **2006**, *6* (3), 371–375.
28. Tsang, S.C.; et al. Immobilization of platinated and iodinated oligonucleotides on carbon nanotubes. Angewandte Chemie International **1997**, *36* (20), 2198–2200.
29. Meng, S.; et al. DNA nucleoside interaction and identification with carbon nanotubes. Nano Lett. **2007**, *7* (1), 45–50.
30. Enyashin, A.N.; Gemming, S.; Seifert, G. DNA-wrapped carbon nanotubes. Nanotechnology **2007**, *18* (24), 245702–245712.
31. Ortmann, F.; Schmidt, W.G.; Bechstedt, F. Attracted by long-range electron correlation: Adenine on graphite. Phy. Rev. Lett. **2005**, *95* (18), 186101–186104.
32. Meng, S.; et al. Determination of DNA-base orientation on carbon nanotubes through directional optical absorbance. Nano Lett. **2007**, *7* (8), 2312–2316.
33. Hughes, M.E.; Brandin, E.; Golovchenko, J.A. Optical absorption of DNA-carbon nanotube structures. Nano Lett. **2007**, *7* (5), 1191–1194.
34. Johnson, R.R.; Johnson, A.T.C.; Klein, M.L. Probing the structure of DNA-carbon nanotube hybrids with molecular dynamics. Nano Lett. **2008**, *8* (1), 69–75.
35. Shtogun, Y.V.; Woods, L.M.; Dovbeshko, G.I. Adsorption of adenine and thymine and their radicals on single-wall carbon nanotubes. J. Phys. Chem. C **2007**, *111* (49), 18174–18181.
36. Lu, Q.; Bhattacharya, B. The role of atomistic simulations in probing small scale aspects of fracture – a case study on a single walled carbon nanotube. Engineering Fracture Mechanics **2005**, *72* (13), 2037–2071.
37. Sreevathsan, R.; et al. Multi-objective materials design by genetic algorithm – Generalized for B1 and B2 ionic structures. Journal of Computational and Theoretical Nanoscience **2009**, *6* (4), 849–856.
38. Sreevathsan, R.; Bhattacharya, B.; Chakraborti, N. Designing of ionic materials through multi-objective genetic algorithms. Materials and Manufacturing Processes **2009**, *24* (2), 162–168.
39. Gao, H.; Kong, Y.; Cui, D. Spontaneous insertion of DNA oligonucleotides into carbon nanotubes. **2003**, *3* (4), 471–473.
40. Lim, M.C.G.; Pei, Q.X.; Zhong, Z.W. Translocation of DNA oligonucleotide through carbon nanotube channels under induced pressure difference. Physica A **2008**, *387* (13), 3111–3120.
41. Lau, E.Y.; Lightstone, F.C.; Colvin, M.E. Dynamics of DNA encapsulated in a hydrophobic nanotube. Chem. Phys. Lett. **2005**, *412* (1–3), 82–87.
42. Okada, T.; et al. Electrically triggered insertion of single-stranded DNA into single-walled carbon nanotubes. Chemical Physics Letters **2006**, *417* (4–6), 288–292.
43. Rajendra, J.; Rodger, A. The binding of single-stranded DNA and PNA to single-walled carbon nanotubes probed by flow linear dichroism. Chem. Eur. J. **2005**, *11* (16), 4841–4847.
44. Manohar, S.; Tang, T.; Jagota, A. Structure of Homopolymer DNA-CNT Hybrids. J. Phys. Chem. C **2007**, *111* (48), 17835–17845.
45. Lu, G.; Maragakis, P.; Kaxiras, E. Carbon nanotube interaction with DNA. Nano Lett. **2005**, *5* (5), 897–900.
46. Martin, W.; Zhu, W.; Krilov, G. Simulation study of noncovalent hybridization of carbon nanotubes by single-stranded DNA in water. J. Phys. Chem. B **2008**, *112* (50), 16076–16089.
47. Lindahl, E.; Hess, B.; Spoel, D.V. GROMACS 3.0: A package for molecular simulation and trajectory analysis. Journal of Molecular Modeling **2001**, *7* (8), 306–317.
48. Bestel, I.; et al. Two-dimensional self-assembly and complementary base-pairing between amphiphile nucleotides on graphite. Journal of Colloid and Interface Science **2008**, *323* (2), 435–440.
49. Mamdouh, W.; et al. Supramolecular nanopatterns self-assembled by adenine-thymine quartets at the liquid/solid interface. J. Am. Chem. Soc. **2006**, *128* (40), 13305–13311.
50. Zhu, N.; et al. Label-free and sequence-specific DNA detection down to a picomolar level with carbon nanotubes as support for probe DNA. Analytica Chimica Acta **2009**, *650* (1), 44–48.
51. Zhou, N.; et al. Highly sensitive electrochemical impedance spectroscopic detection of DNA hybridization based on Aunano–CNT/PAN nano films. Talanta **2009**, *77* (3), 1021–1026.
52. Li, Z.; Wu, Z.; Li, K. The high dispersion of DNA-multiwalled carbon nanotubes and their properties. Analytical Biochemistry **2009**, *387*, 267–270.
53. Guo, M.; et al. Electrochemical characteristics of the immobilization of calf thymus DNA molecules on multi-walled carbon nanotubes. Bioelectrochemistry **2004**, *62* (1), 29–35.
54. Berti, F.; et al. Aligned carbon nanotube thin films for DNA electrochemical sensing. Electrochimica Acta **2009**, *54* (22), 5035–5041.
55. Qi, H.; et al. Electrochemical detection of DNA hybridization based on polypyrrole/ss-DNA/multi-wall carbon nanotubes paste electrode. Talanta **2007**, *72* (3), 1030–1035.
56. Zheng, M.; Rostovtsev, V.V. Photoinduced charge transfer mediated by DNA-wrapped carbon nanotubes. J. Am. Chem. Soc. **2006**, *128* (24), 7702–7703.

57. Dai, H.; et al. Electrical transport properties and field-effect transistors of carbon nanotubes. NANO: Brief Reports and Reviews **2006**, *1* (1), 1–4.
58. Napier, M.E.; Hull, D.O.; Thorp, H.H. Electrocatalytic oxidation of DNA-wrapped carbon nanotubes. J. Am. Chem. Soc. **2005**, *127* (34), 11952–11953.
59. Hembrama, K.P.S.S.; Rao, G.M. Studies on CNTs/DNA composite. Materials Sc. and Engineering: C **2008**, *29* (4), 1093–1097.
60. Wang, G.; Xu, J.J.; Chen, H.Y. Interfacing cytochrome c to electrodes with a DNA – carbon nanotube composite film. Electrochemistry Communications **2002**, *4* (6), 506–509.
61. Basuray, S.; et al. Shear and AC field enhanced carbon nanotube impedance assay for rapid, sensitive, and mismatch-discriminating DNA hybridization. ACS Nano **2009**, *3* (7), 1823–1830.
62. Zhang, L.; et al. Optical characterizations and electronic devices of nearly pure (10, 5) single-walled carbon nanotubes. J. Am. Chem. Soc. **2009**, *131* (7), 2454–2455.
63. Zhang, L.; et al. Assessment of chemically separated carbon nanotubes for nanoelectronics. J. Am. Chem. Soc. **2008**, *130* (8), 2686–2691.
64. Kim, S.N.; et al. Enrichment of (6, 5) single wall carbon nanotubes using genomic DNA. Nano Lett. **2008**, *8* (12), 4415–4420.
65. Cha, M.; et al. Reversible metal-semiconductor transition of ssDNA-decorated single-walled carbon nanotubes. Nano Lett. **2009**, *9* (4), 1345–1349.
66. Malik, S.; et al. Physical chemical characterization of DNA-SWNT suspensions and associated composites. Composites Science and Technology **2007**, *67* (5), 916–921.
67. Simmons, T.J.; et al. Noncovalent functionalization as an alternative to oxidative acid treatment of single wall carbon nanotubes with applications for polymer composites. ACS Nano **2009**, *3* (4), 865–870.
68. Badaire, S.; et al. Liquid crystals of DNA stabilised carbon nanotubes. Adv. Mater. **2005**, *17*, 1673–1676.
69. Hazani, M.; et al. Confocal fluorescence imaging of DNA-functionalized carbon nanotubes. Nano Lett. **2003**, *3* (2), 153–155.
70. Mizutani, T.; et al. Mechanism of induced circular dichroism of amino acid ester-porphyrin supramolecular systems. Implications to the origin of the circular dichroism of hemoprotein. Inorg. Chem. **1994**, *33*, 3558–3566.
71. Gao, X.; et al. Detection of trace Hg^{2+} via induced circular dichroism of DNA wrapped around single-walled carbon nanotubes. J. Am. Chem. Soc. **2008**, *130*, 9190–9191.
72. Dovbeshko, G.I.; et al. DNA interaction with single-walled carbon nanotubes: a SEIRA study. Chem. Phys. Lett. **2003**, *372* (3–4), 432–437.
73. Yarotski, D.A.; et al. Scanning tunneling microscopy of DNA-wrapped carbon nanotubes. Nano Lett. **2009**, *9* (1), 12–17.
74. Campbell, J.F.; et al. Atomic force microscopy studies of DNA-wrapped carbon nanotube structure and binding to quantum dots. J. Am. Chem. Soc. **2008**, *130* (30), 10648–10655.
75. Burns, D.J.; Toumi, K.Y. Shortening carbon nanotube-tipped AFM probes. International Journal of Nanomanufacturing **2007**, *1* (6), 799–809.
76. Burns, D.J.; Toumi, K.Y. Measuring, shortening and functionalizing carbon nanotube tipped AFM probes for DNA sequencing. SMA symposium, 2007.
77. Gigliotti, B.; et al. Sequence-independent helical wrapping of single-walled carbon nanotubes by long genomic DNA. Nano Lett. **2006**, *6* (2), 159–164.
78. Buzaneva, E.; et al. DNA nanotechnology of carbon nanotube cells: Physico-chemical models of self-organization and properties. Mater. Sci. Eng. C **2002**, *19* (1–2), 41–45.
79. Huang, X.; Mclean, R.S.; Zheng, M. High-resolution length sorting and purification of DNA-wrapped carbon nanotubes by size-exclusion chromatography. Analytical Chemistry **2005**, *77* (19), 6225–6228.
80. Nepal, D.; et al. Supramolecular conjugates of carbon nanotubes and DNA by a solid-state reaction. Biomacromolecules **2005**, *6* (6), 2919–2922.
81. Ajayan, P.M.; Iijima, S.; Ichihashi, T. Electron energy-loss spectroscopy of carbon nanometer-size tubes. Phy. Rev. B **1993**, *47* (11), 6859–6862.
82. Strano, M.S.; et al. Understanding the nature of the DNA-assisted separation of single-walled carbon nanotubes using fluorescence and Raman spectroscopy. Nano. Lett. **2004**, *4* (4), 543–550.
83. Strano, M.S. Probing chiral selective reactions using a revised Kataura plot for the interpretation of single-walled carbon nanotube spectroscopy. J. Am. Chem. Soc. **2003**, *125* (51), 16148–16153.
84. Rajendra, J.; et al. Flow linear dichroism to probe binding of aromatic molecules and DNA to single-walled carbon nanotubes. J. Am. Chem. Soc. **2004**, *126* (36), 11182–11188.
85. Zheng, M.; et al. Structure-based carbon nanotube sorting by sequence-dependent DNA assembly. Science **2003**, *302* (5650), 1545–1548.
86. Dukovic, G.; et al. Racemic single-walled carbon nanotubes exhibit circular dichroism when wrapped with DNA. J. Am. Chem. Soc. **2006**, *128* (28), 9004–9005.
87. Martinez, M.T.; et al. Label-free DNA biosensors based on functionalized carbon nanotube field effect transistors. Nano Lett. **2009**, *9* (2), 530–536.
88. Dong, X.; et al. Label-free electronic detection of DNA using simple double-walled carbon nanotube resistors. J. Phys. Chem. C **2008**, *112* (26), 9891–9895.
89. Ma, Y.; et al. The electronic role of DNA-functionalized carbon nanotubes: efficacy for in situ polymerization of conducting polymer nanocomposites. J. Am. Chem. Soc. **2008**, *130* (25), 7921–7928.
90. Talin, A.A.; et al. Assembly and electrical characterization of DNA-wrapped carbon nanotube devices. J. Vac. Sc. Tech. B **2004**, *22* (6), 3107–3111.
91. Staii, C.; Alan, J.; Johnson, T. DNA-decorated carbon nanotubes for chemical sensing. Nano Lett. **2005**, *5* (9), 1774–1778.
92. Star, A.; et al. Label-free detection of DNA hybridization using carbon nanotube network field-effect transistors. Biophysics **2006**, *103* (4), 921–926.
93. Tang, X.; et al. Carbon nanotube DNA sensor and sensing mechanism. Nano Lett. **2006**, *6* (8), 1632–1636.